Efficient one-pot synthesis of [3]catenanes based on Pt(II) metallacycles with a flexible building block

Yuan-Guang Shao,[a] Lang He,[a] Qian-Qian Mao,[a] Tao Hong,[a] Xin-Wen Ying,[a]
Zibin Zhang,[a] Shijun Li*[a] and Peter J. Stang*[b]

[a]*College of Material, Chemistry and Chemical Engineering, Hangzhou Normal University, Hangzhou 311121, P. R. China*

[b]*Department of Chemistry, University of Utah, 315 South 1400 East, Room 2020, Salt Lake City, Utah 84112*

Email address: l_shijun@hznu.edu.cn; stang@chem.utah.edu

Table of Contents

*1. ^{1}H NMR, ^{13}C NMR and mass spectra of **1a***

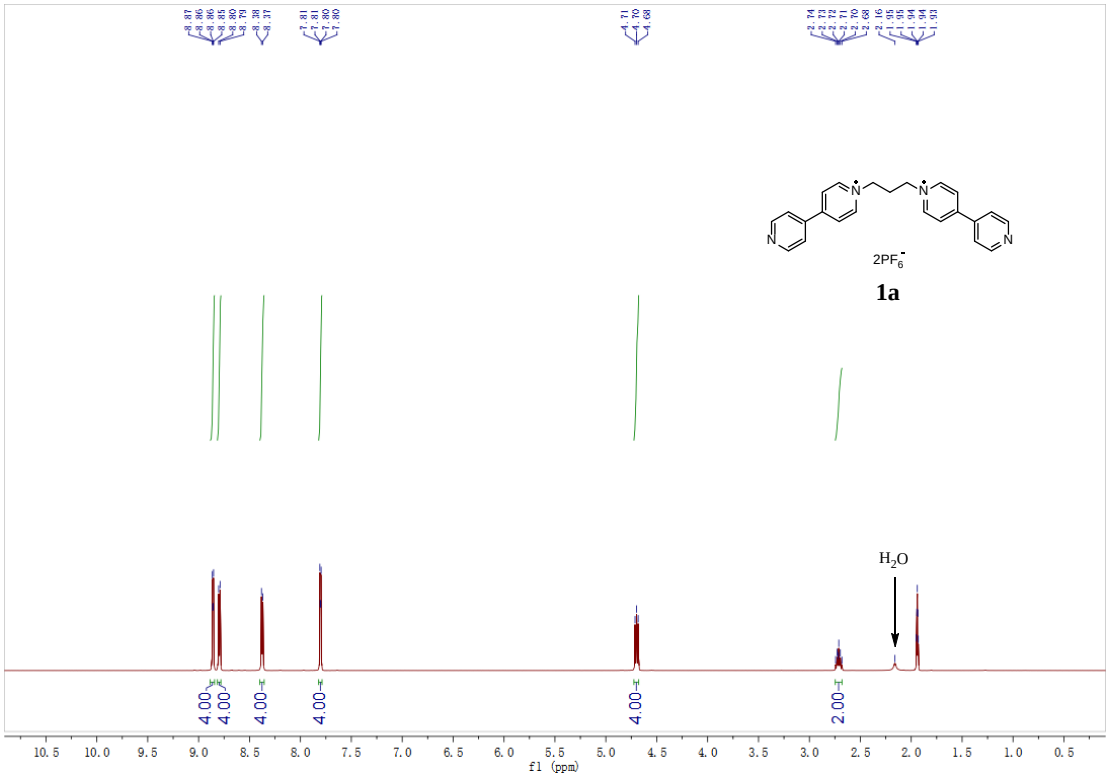

Fig. S1 ^{1}H NMR (500 MHz, CD_3CN, 25 °C) spectrum of **1a**.

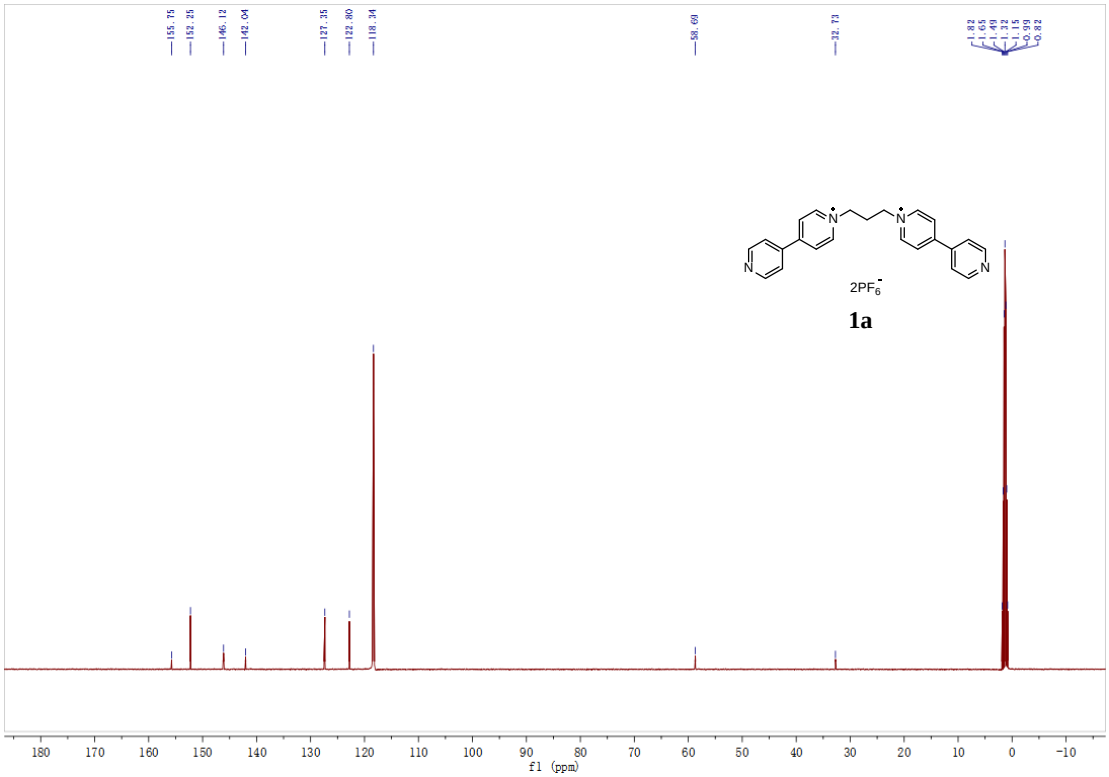

Fig. S2 ^{13}C{^{1}H} NMR (126 MHz, CD_3CN, 25 °C) spectrum of **1a**.

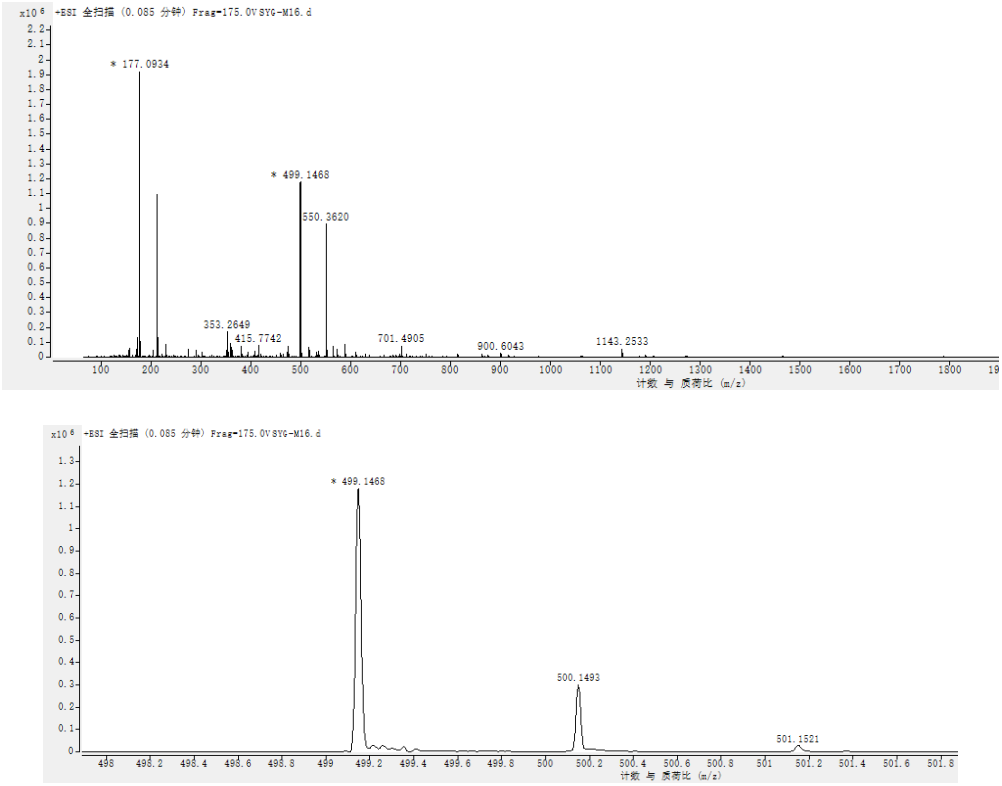

Fig. S3 High resolution electrospray ionization mass spectrum of **1a**. *m*/*z* calcd. for $C_{23}H_{22}F_6N_4P$ ([M – PF_6]$^+$), 499.1481; found, 499.1468, error –2.6 ppm.

2. ^{1}*H NMR spectrum of* ***1b***

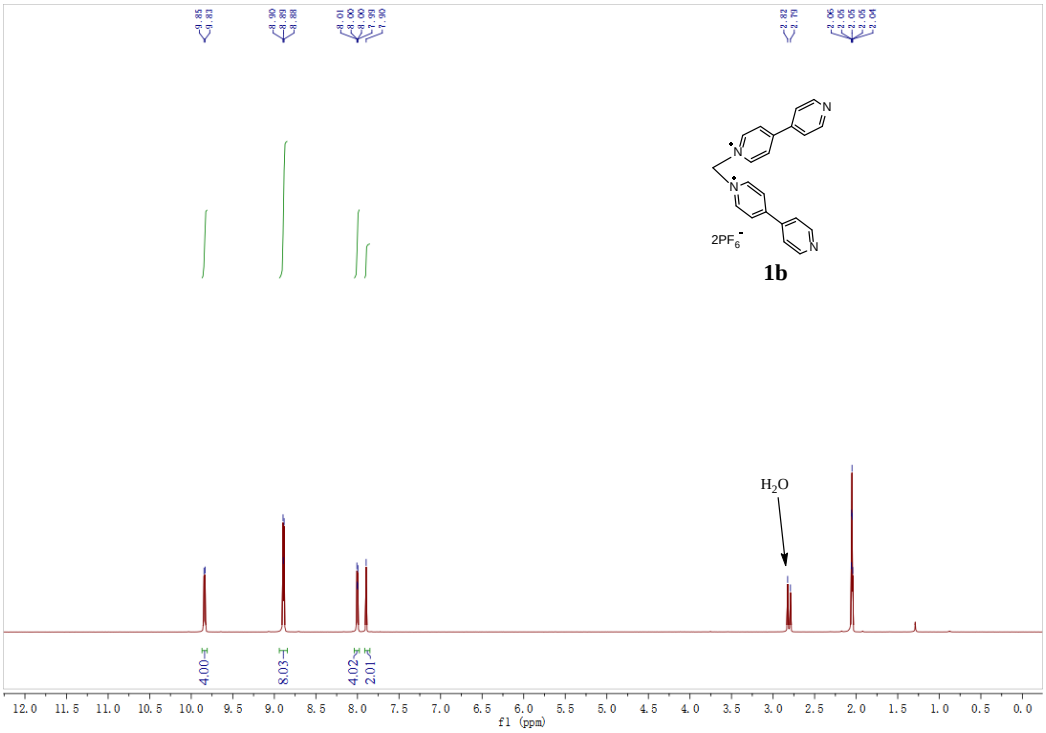

Fig. S4 ^{1}H NMR (500 MHz, acetone-d_6, 25 °C) spectrum of **1b**.

*3. ^{1}H NMR, ^{31}P NMR and ^{1}H-^{1}H COSY NMR spectra of metallacycles **2a** and **2b***

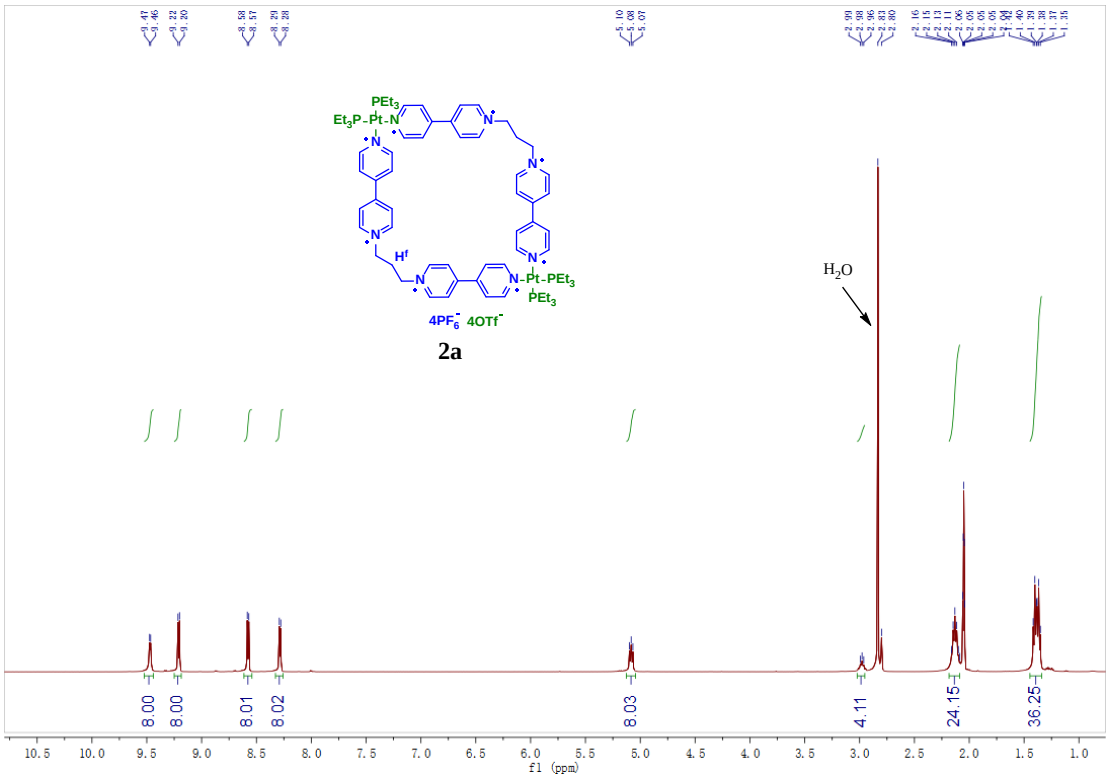

Fig. S5 ^{1}H NMR (500 MHz, acetone-d_6, 25 °C) spectrum of metallacycle **2a**.

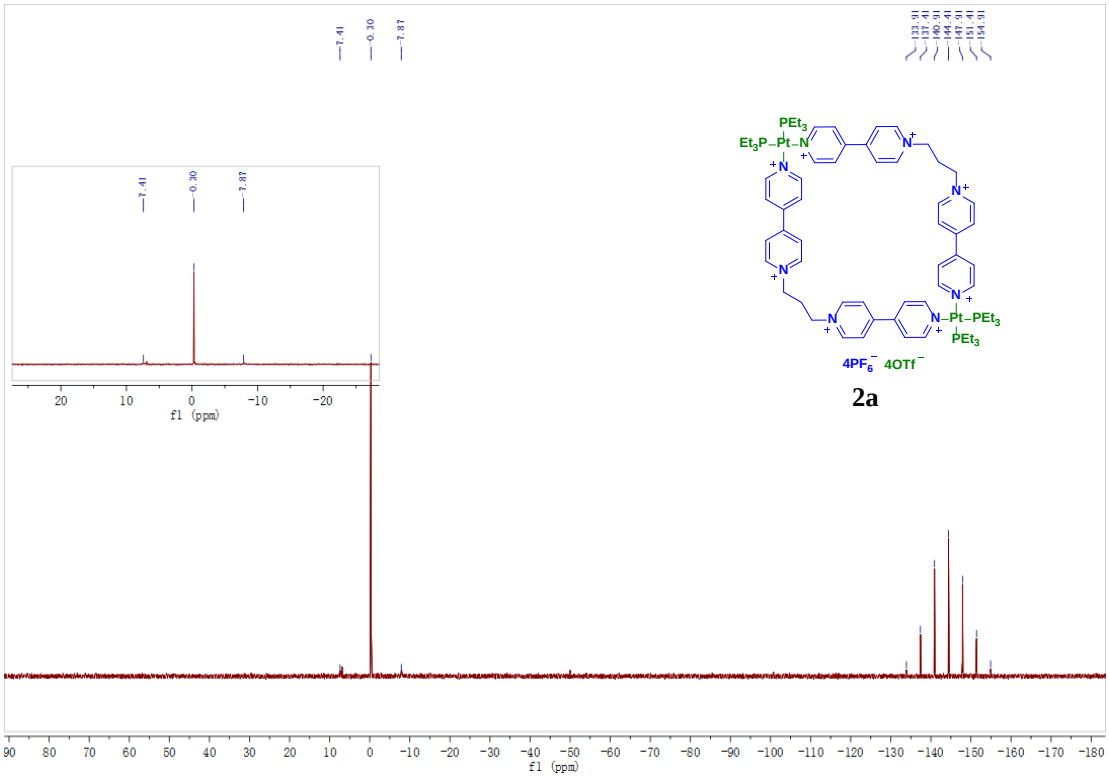

Fig. S6 ^{31}P{^{1}H} NMR (202 MHz, acetone-d_6, 25 °C) spectrum of metallacycle **2a**.

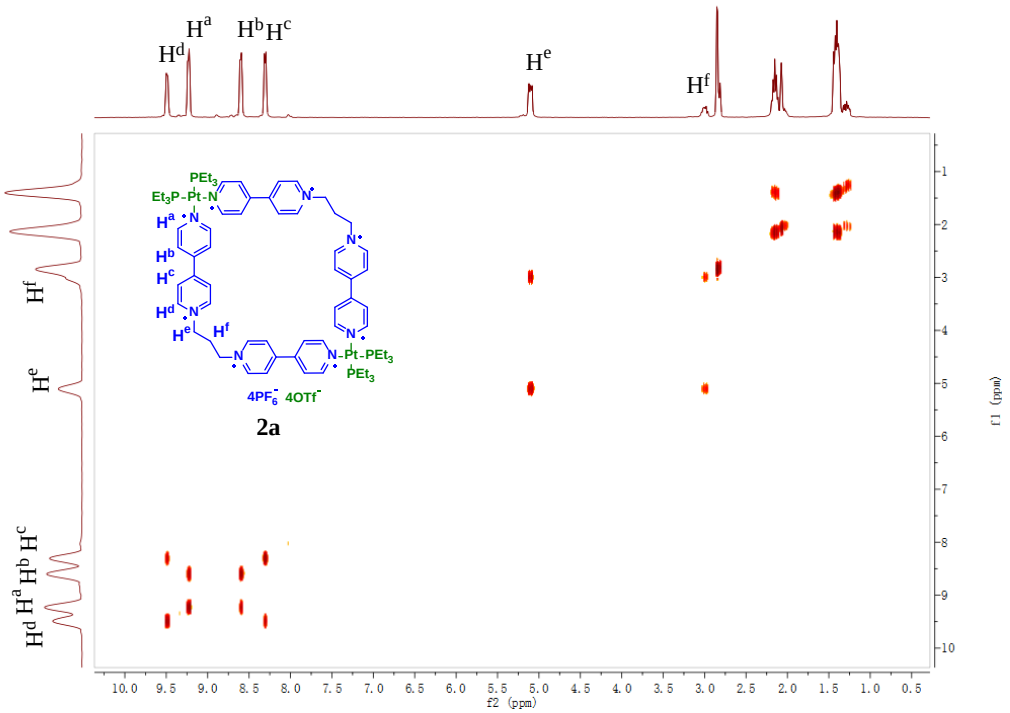

Fig. S7 ^{1}H-^{1}H COSY NMR (500 MHz, acetone-d_6, 25 °C) spectrum of metallacycle **2a**.

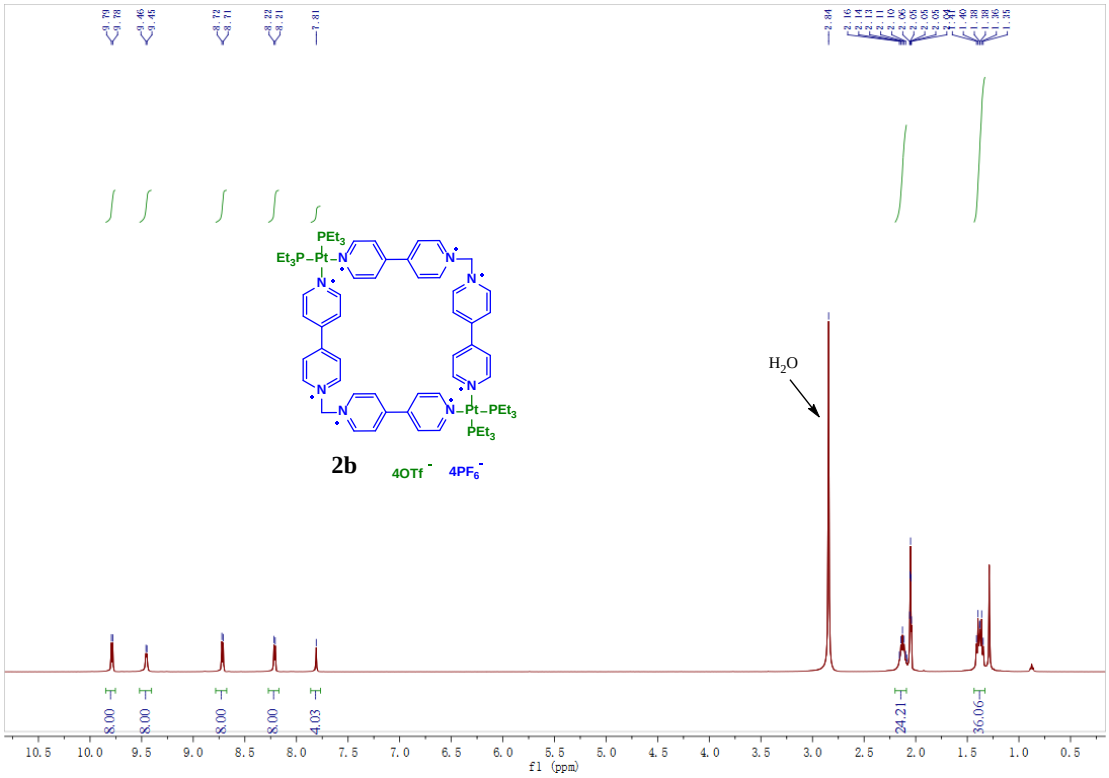

Fig. S8 ^{1}H NMR (500 MHz, acetone-d_6, 25 °C) spectrum of metallacycle **2b**.

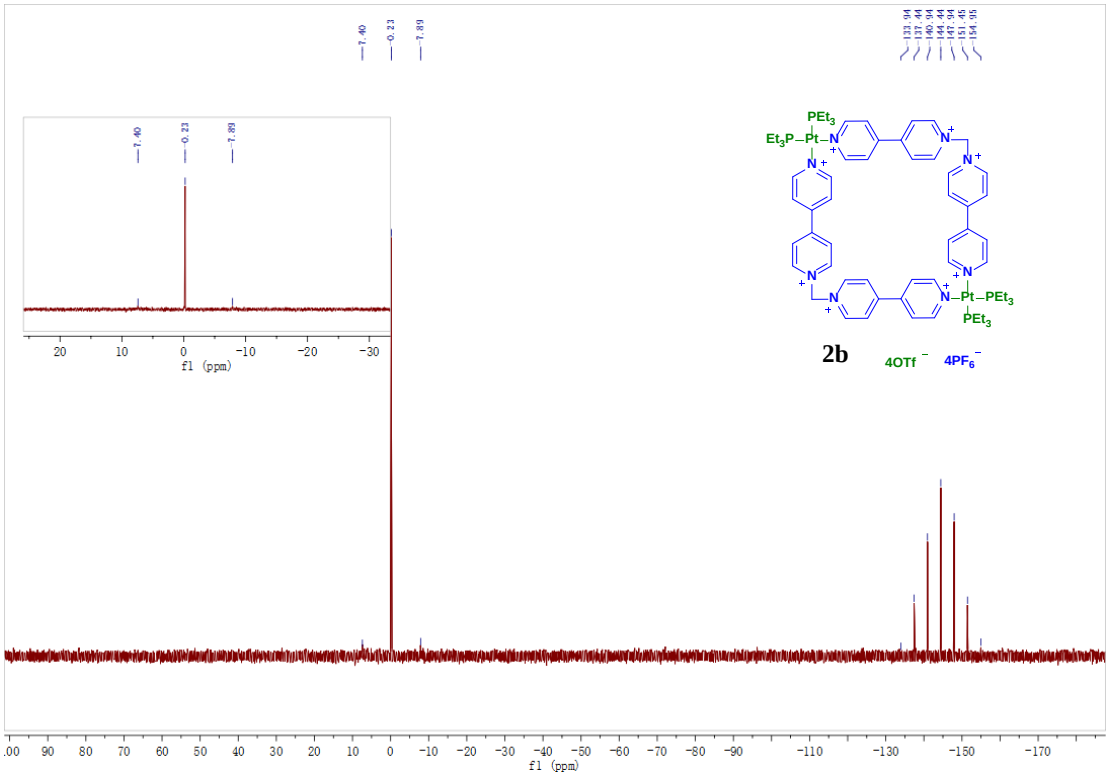

Fig. S9 $^{31}P\{^{1}H\}$ NMR (202 MHz, acetone-d_6, 25 °C) spectrum of metallacycle **2b**.

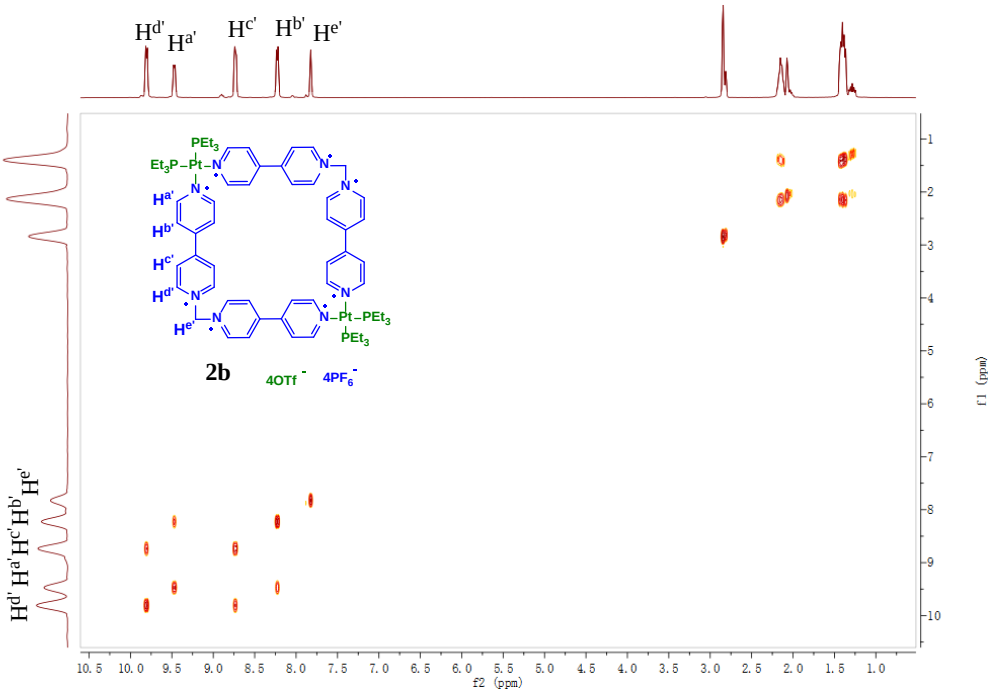

Fig. S10 ^{1}H-^{1}H COSY NMR (500 MHz, acetone-d_6, 25 °C) spectrum of metallacycle **2b**.

*4. ^{1}H NMR and ^{31}P NMR spectra of [3]catenane **3**, [3]catenane **4** and [3]catenane **5***

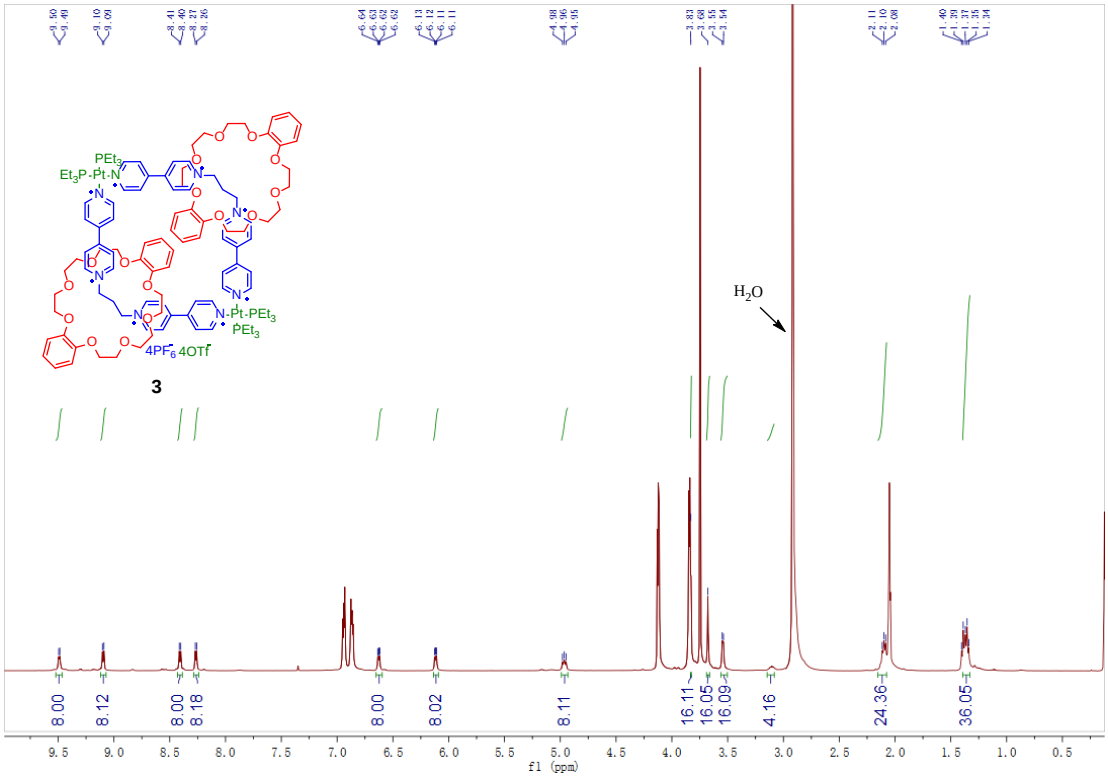

Fig. S11 ^{1}H NMR (500 MHz, acetone-d_6, 25 °C) spectrum of [3]catenane **3**.

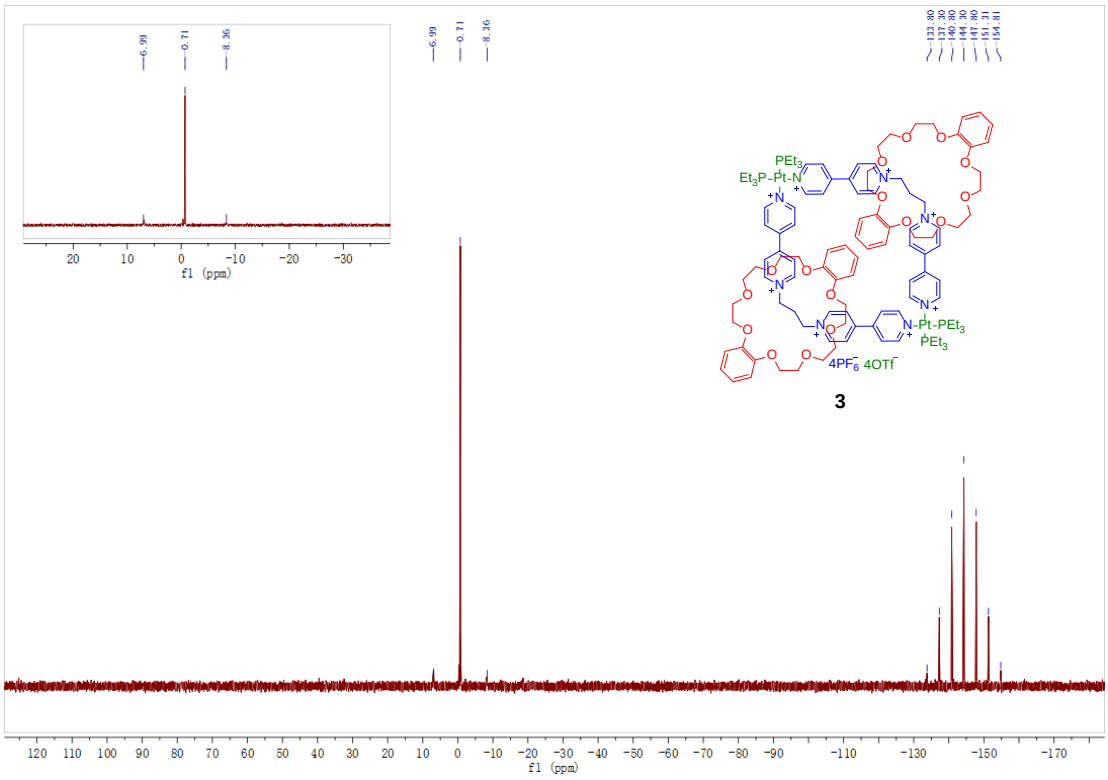

Fig. S12 ^{31}P{^{1}H} NMR (202 MHz, acetone-d_6, 25 °C) spectrum of [3]catenane **3**.

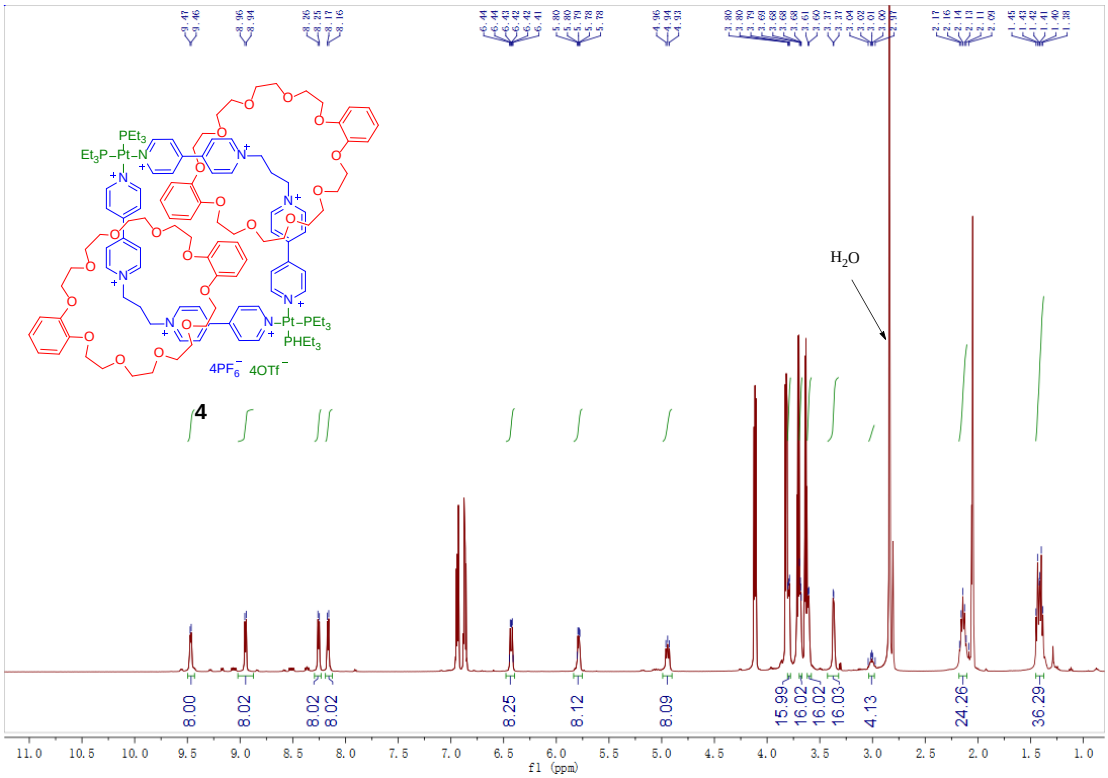

Fig. S13 ^{1}H NMR (500 MHz, acetone-d_6, 25 °C) spectrum of [3]catenane **4**.

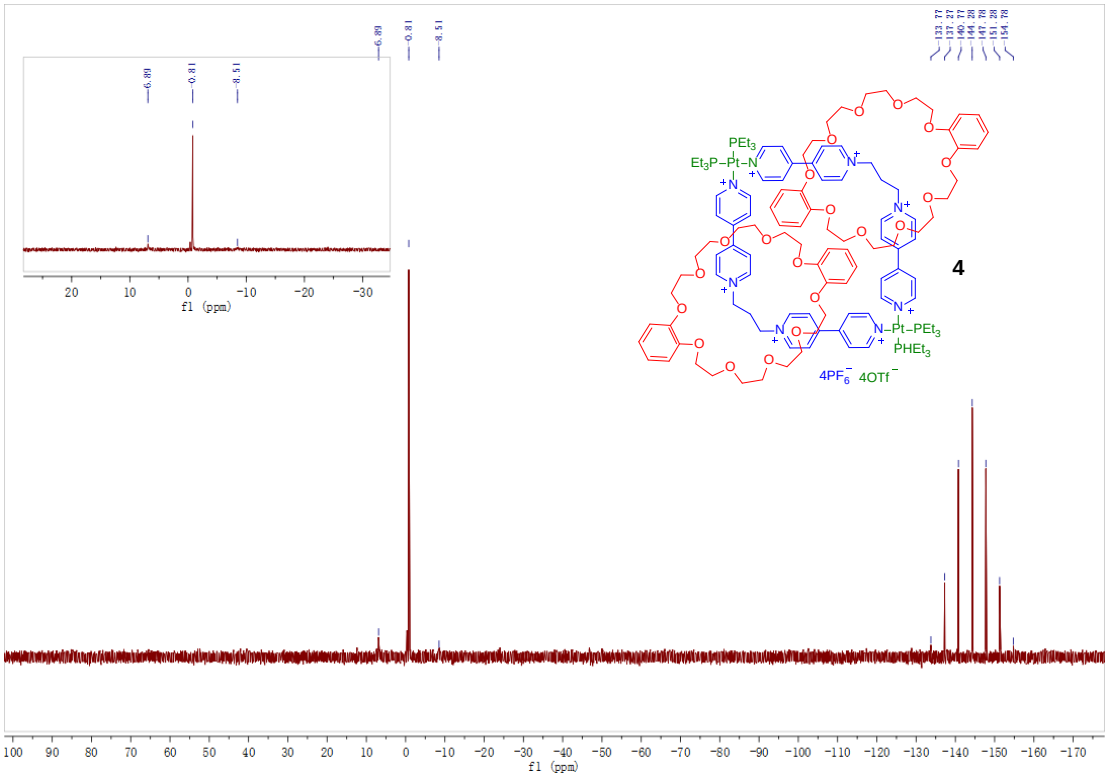

Fig. S14 ^{31}P{^{1}H} NMR (202 MHz, acetone-d_6, 25 °C) spectrum of [3]catenane **4**.

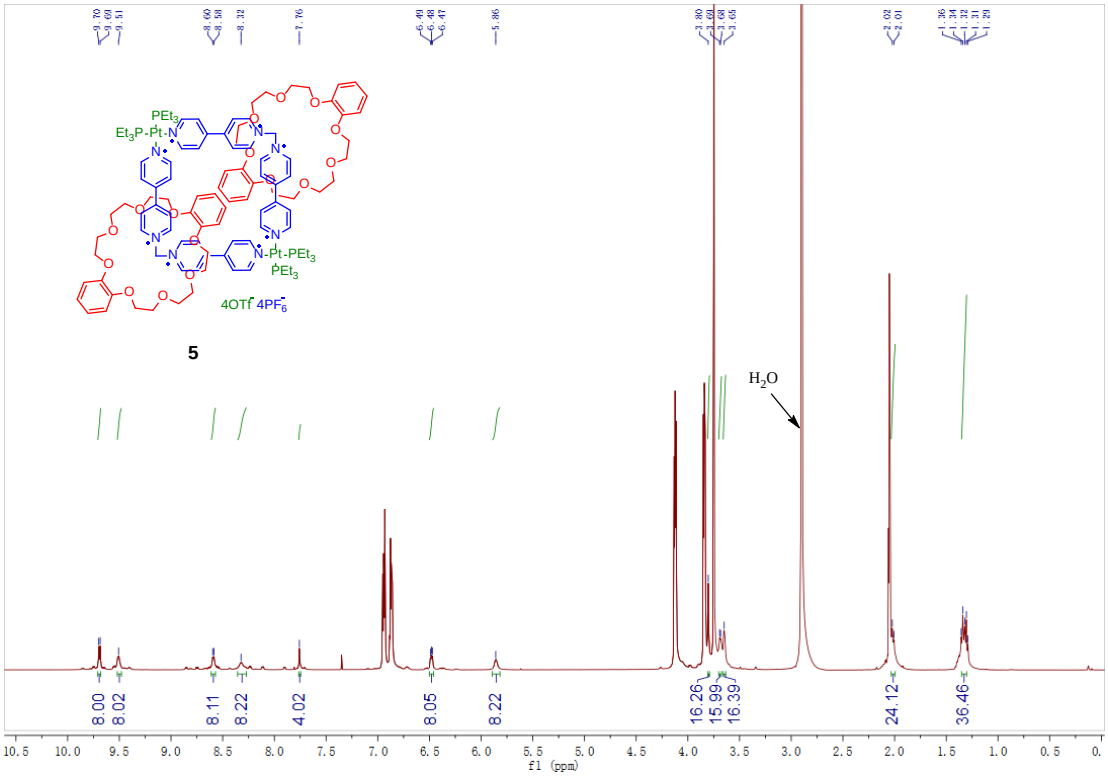

Fig. S15 ^{1}H NMR (500 MHz, acetone-d_6, 25 °C) spectrum of [3]catenane **5**.

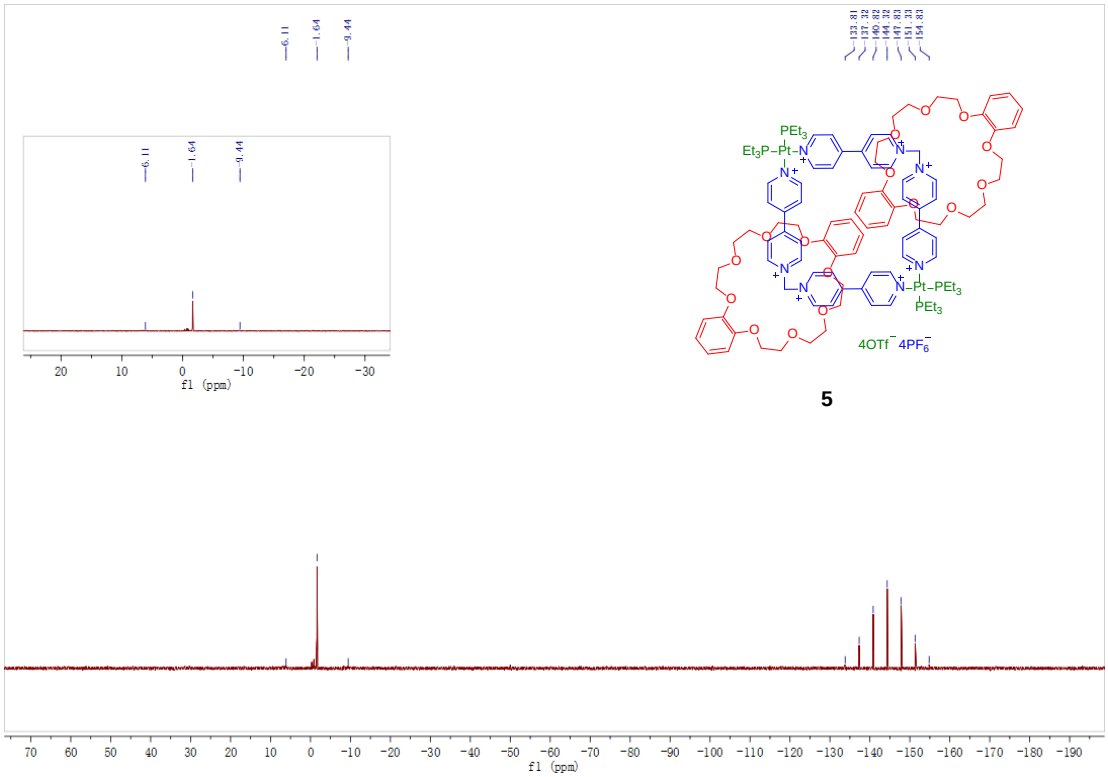

Fig. S16 ^{31}P{^{1}H} NMR (202 MHz, acetone-d_6, 25 °C) spectrum of [3]catenane **5**.

*5. ESI-MS spectra of metallacycles **2a** and **2b***

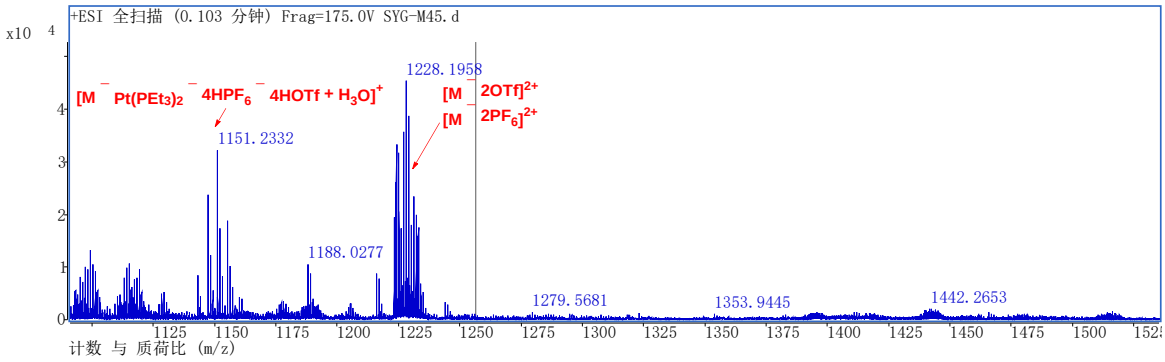

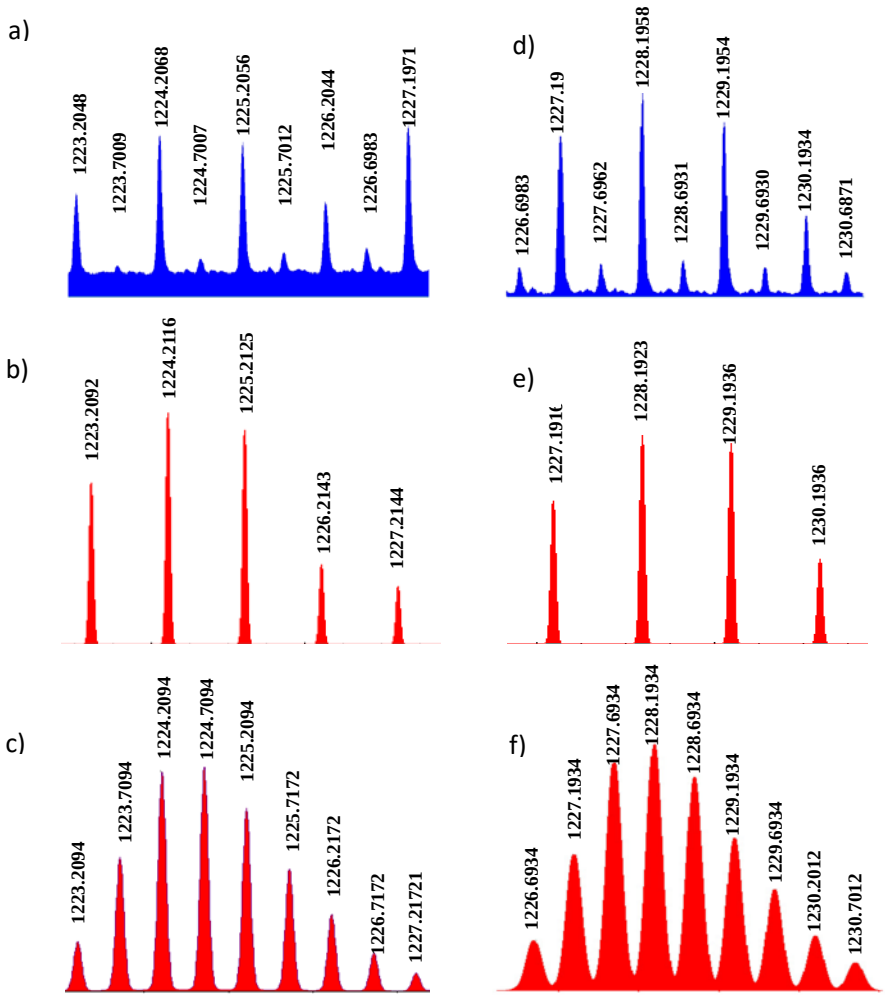

Fig. S17 ESI-MS spectrum of **2a**. a) experimental spectrum of [**2a** – 2OTf]$^{2+}$ (*m/z* = 1224.2068) and its fragment [**1a** + **6** – OTf]$^{+}$ (*m/z* = 1224.2068); b) simulated spectrum of the fragment [**1a** + **6** – OTf]$^{+}$; c) simulated spectrum of [**2a** – 2OTf]$^{2+}$; d) experimental spectrum of [**2a** – 2PF$_6$]$^{2+}$ (*m/z* = 1228.1958) and its fragment [**1a** + **6** – PF$_6$]$^{+}$ (*m/z* = 1228.1958); e) simulated spectrum of the fragment [**1a** + **6** – PF$_6$]$^{+}$; f) simulated spectrum of [**2a** – 2PF$_6$]$^{2+}$.

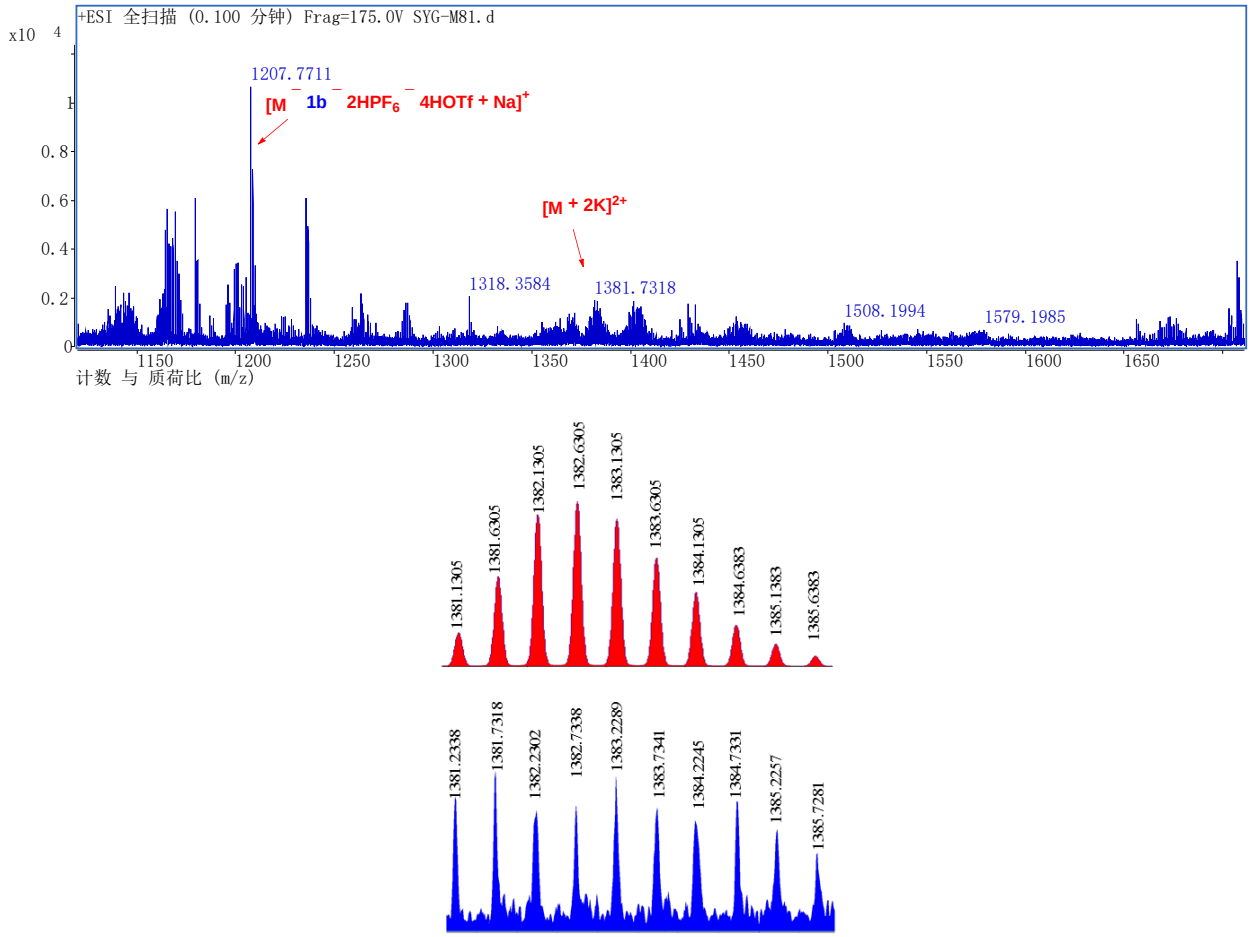

Fig. S18 ESI-MS spectrum of [**2b** + 2K]$^{2+}$ (*m*/*z* = 1383.2289) (blue), and its simulated spectrum (red).

*6. ESI-MS spectra of [3]catenane **3**, [3]catenane **4** and [3]catenane **5***

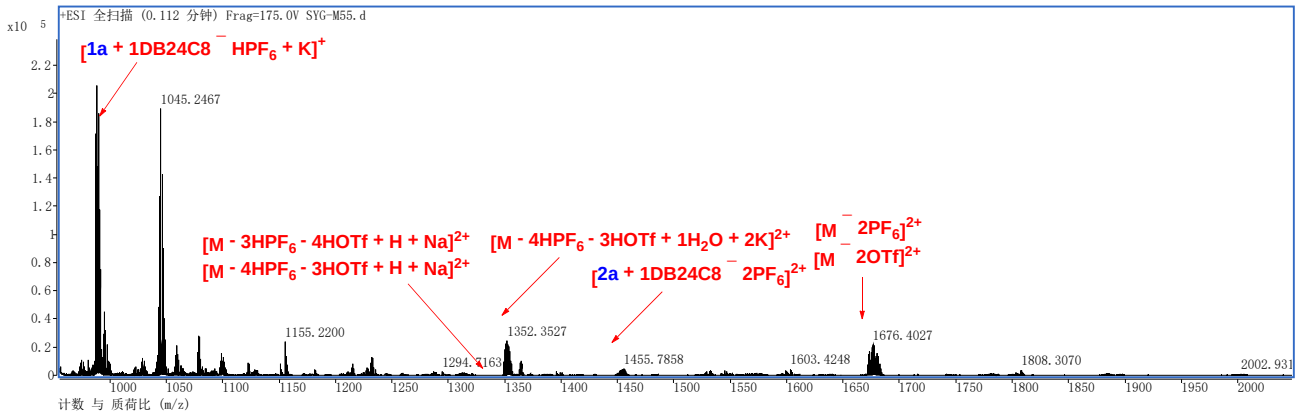

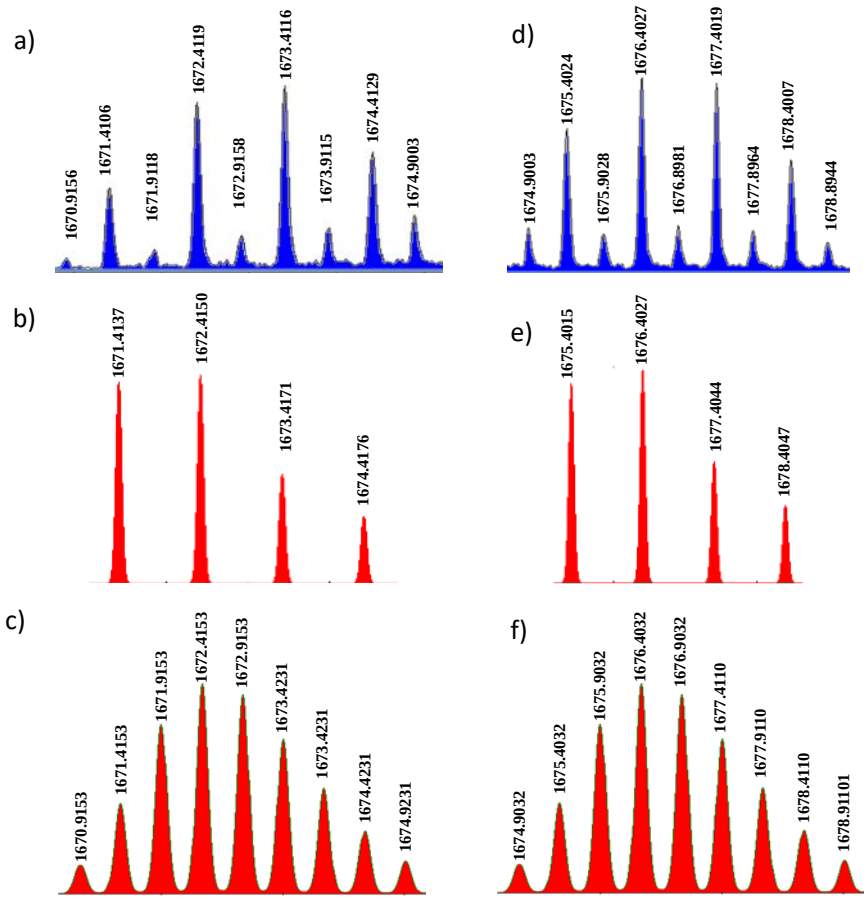

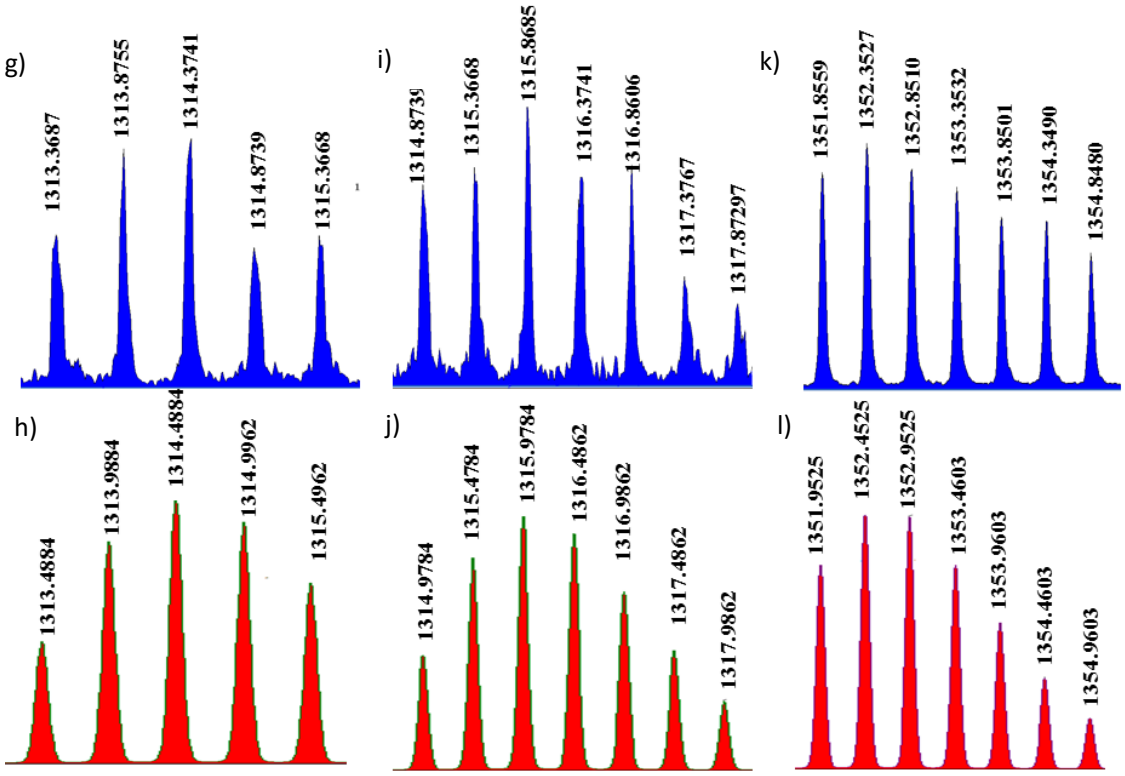

Fig. S19 ESI-MS spectrum of **3**. a) experimental spectrum of [**3** – 2OTf]$^{2+}$ (*m*/*z* = 1672.4119) and its fragment [**1a** + **6** + DB24C8 – OTf]$^{+}$ (*m*/*z* = 1672.4119); b) simulated spectrum of the fragment [**1a** + **6** + DB24C8 – OTf]$^{+}$; c) simulated spectrum of [**3** – 2OTf]$^{2+}$; d) experimental spectrum of [**3** – 2PF_6]$^{2+}$ (*m*/*z* = 1676.4027) and its fragment [**1a** + **6** + DB24C8 – PF_6]$^{+}$ (*m*/*z* = 1676.4027); e) simulated spectrum of the fragment [**1a** + **6** + DB24C8 – PF_6]$^{+}$; f) simulated spectrum of [**3** – 2PF_6]$^{2+}$; g) experimental spectrum of [**3** – 3HPF_6 – 4HOTf + H + Na]$^{2+}$ (*m*/*z* = 1314.3741); h) simulated spectrum of [**3** – 3HPF_6 – 4HOTf + H + Na]$^{2+}$ (*m*/*z* = 1314.4884); i) experimental spectrum of [**3** – 4HPF_6 – 3HOTf + H + Na]$^{2+}$ (*m*/*z* = 1316.3741); j) simulated spectrum of [**3** – 4HPF_6 – 3HOTf + H + Na]$^{2+}$ (*m*/*z* = 1316.4862); k) experimental spectrum of [**3** – 4HPF_6 – 3HOTf + 1H_2O + 2K]$^{2+}$ (*m*/*z* = 1352.8510); l) simulated spectrum of [**3** – 4HPF_6 – 3HOTf + 1H_2O + 2K]$^{2+}$ (*m*/*z* = 1352.9525).

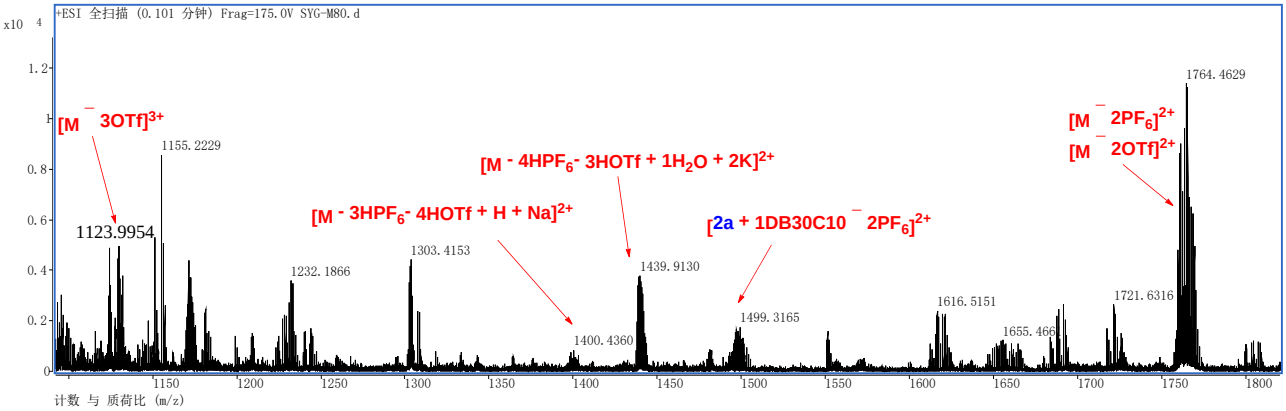
+ESI 全扫描 (0.101 分钟) Frag=175.0V SYG-M80.d
x10 4
[M − 3OTf]3+
1155.2229
1123.9954
1232.1866
1303.4153
[M - 3HPF6- 4HOTf + H + Na]2+
1400.4360
[M - 4HPF6- 3HOTf + 1H2O + 2K]2+
1439.9130
[2a + 1DB30C10 − 2PF6]2+
1499.3165
1616.5151
1655.466
1721.6316
[M − 2PF6]2+
[M − 2OTf]2+
1764.4629
计数 与 质荷比 (m/z)

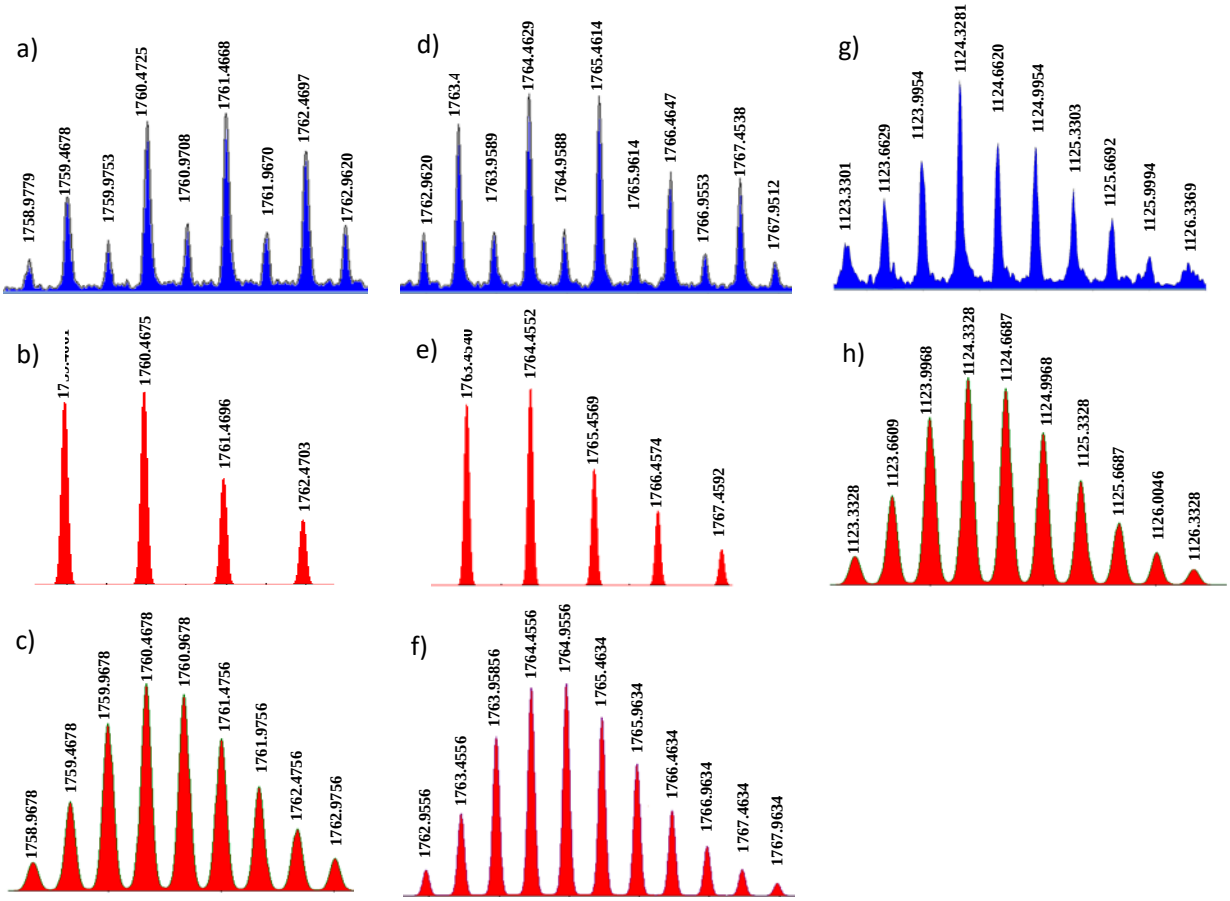
a)
1758.9779
1759.4678
1759.9753
1760.4725
1760.9708
1761.4668
1761.9670
1762.4697
1762.9620
b)
1760.4675
1761.4696
1762.4703
c)
1758.9678
1759.4678
1759.9678
1760.4678
1760.9678
1761.4756
1761.9756
1762.4756
1762.9756
d)
1762.9620
1763.4
1763.9589
1764.4629
1764.9588
1765.4614
1765.9614
1766.4647
1766.9553
1767.4538
1767.9512
e)
1764.4552
1765.4569
1766.4574
1767.4592
f)
1762.9556
1763.4556
1763.95856
1764.4556
1764.9556
1765.4634
1765.9634
1766.4634
1766.9634
1767.4634
1767.9634
g)
1123.3301
1123.6629
1123.9954
1124.3281
1124.6620
1124.9954
1125.3303
1125.6692
1125.9994
1126.3369
h)
1123.3328
1123.6609
1123.9968
1124.3328
1124.6687
1124.9968
1125.3328
1125.6687
1126.0046
1126.3328

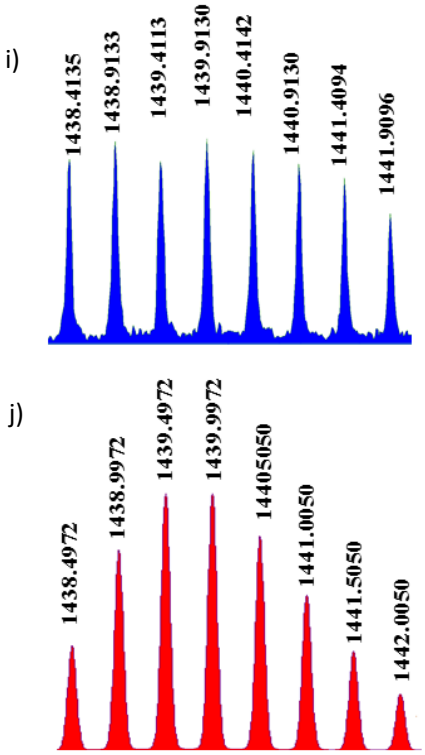

Fig. S20 ESI-MS spectrum of **4**. a) experimental spectrum of [**4** – 2OTf]$^{2+}$ (*m*/*z* = 1760.4725) and its fragment [**1a** + **6** + DB30C10 – OTf]$^{+}$ (*m*/*z* = 1760.4725); b) simulated spectrum of the fragment [**1a** + **6** + DB30C10 – OTf]$^{+}$; c) simulated spectrum of [**4** – 2OTf]$^{2+}$; d) experimental spectra of [**4** – 2PF$_6$]$^{2+}$ (*m*/*z* = 1764.4629) and its fragment [**1a** + **6** + DB30C10 – PF$_6$]$^{+}$ (*m*/*z* = 1764.4629); e) simulated spectrum of the fragment [**1a** + **6** + DB30C10 – PF$_6$]$^{+}$; f) simulated spectrum of [**4** – 2PF$_6$]$^{2+}$; g) experimental spectrum of [**4** – 3OTf]$^{3+}$ (*m*/*z* = 1123.9954); h) simulated spectrum of [**4** – 3OTf]$^{3+}$; i) experimental spectrum of [**4** – 4HPF$_6$ – 3HOTf + 1H$_2$O + 2K]$^{2+}$ (*m*/*z* = 1440.4142); j) simulated spectrum of [**4** – 4HPF$_6$ – 3HOTf + 1H$_2$O + 2K]$^{2+}$ (*m*/*z* = 1440.5050).

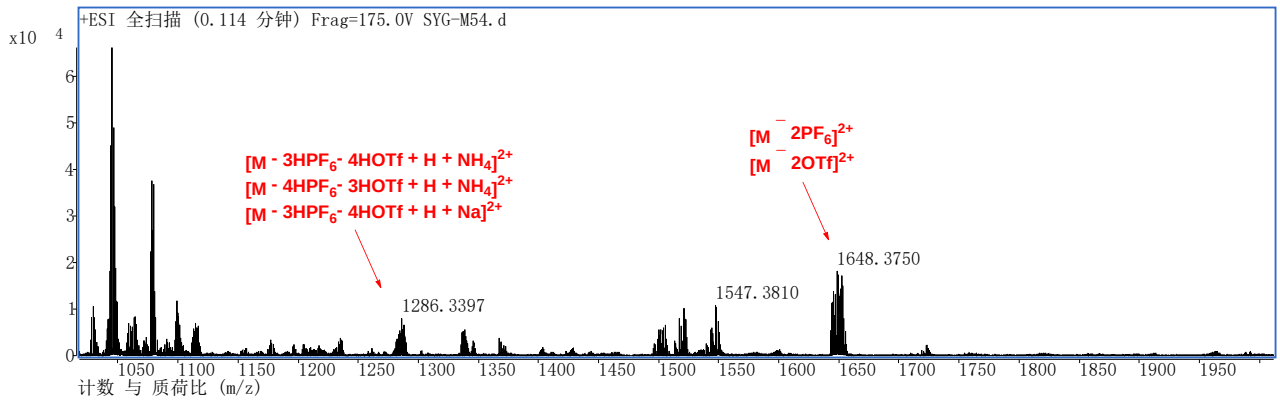

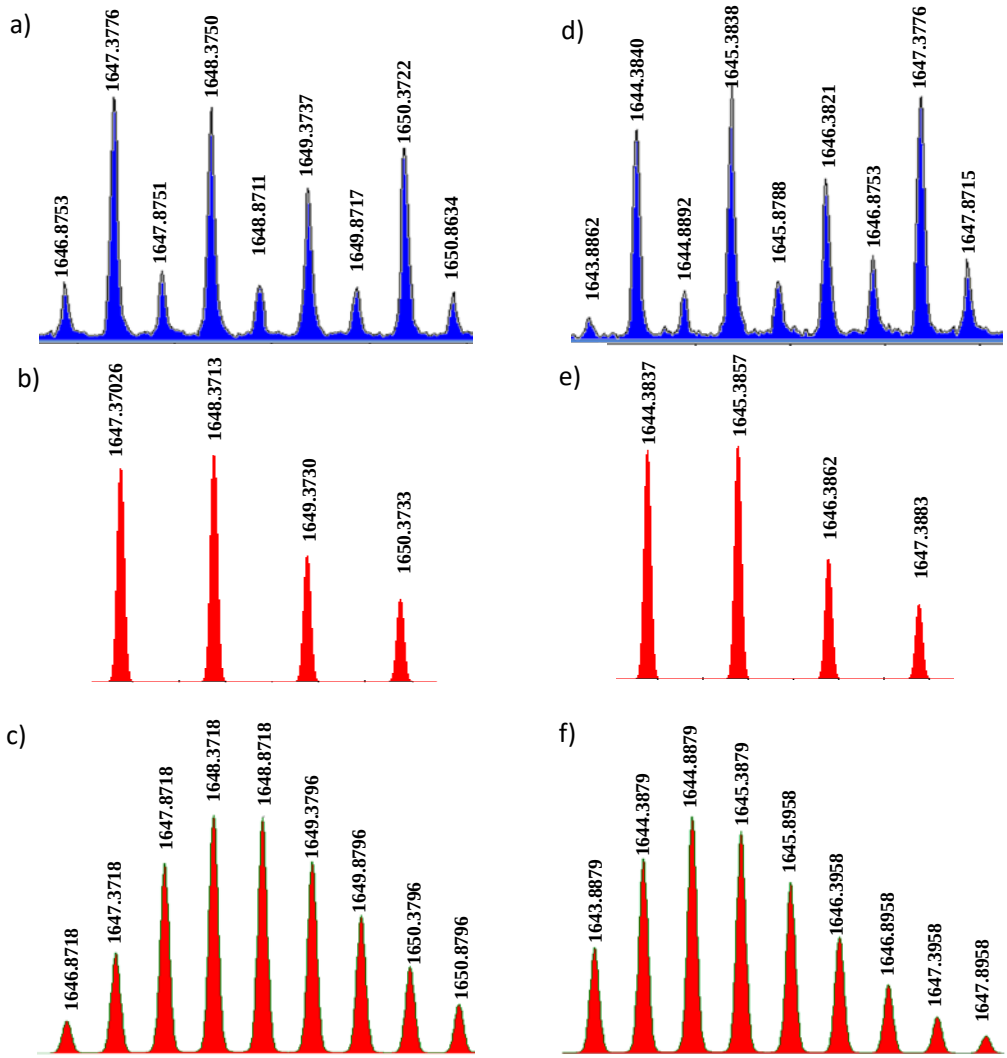
a)
1646.8753
1647.3776
1647.8751
1648.3750
1648.8711
1649.3737
1649.8717
1650.3722
1650.8634
b)
1647.37026
1648.3713
1649.3730
1650.3733
c)
1646.8718
1647.3718
1647.8718
1648.3718
1648.8718
1649.3796
1649.8796
1650.3796
1650.8796
d)
1643.8862
1644.3840
1644.8892
1645.3838
1645.8788
1646.3821
1646.8753
1647.3776
1647.8715
e)
1644.3837
1645.3857
1646.3862
1647.3883
f)
1643.8879
1644.3879
1644.8879
1645.3879
1645.8958
1646.3958
1646.8958
1647.3958
1647.8958

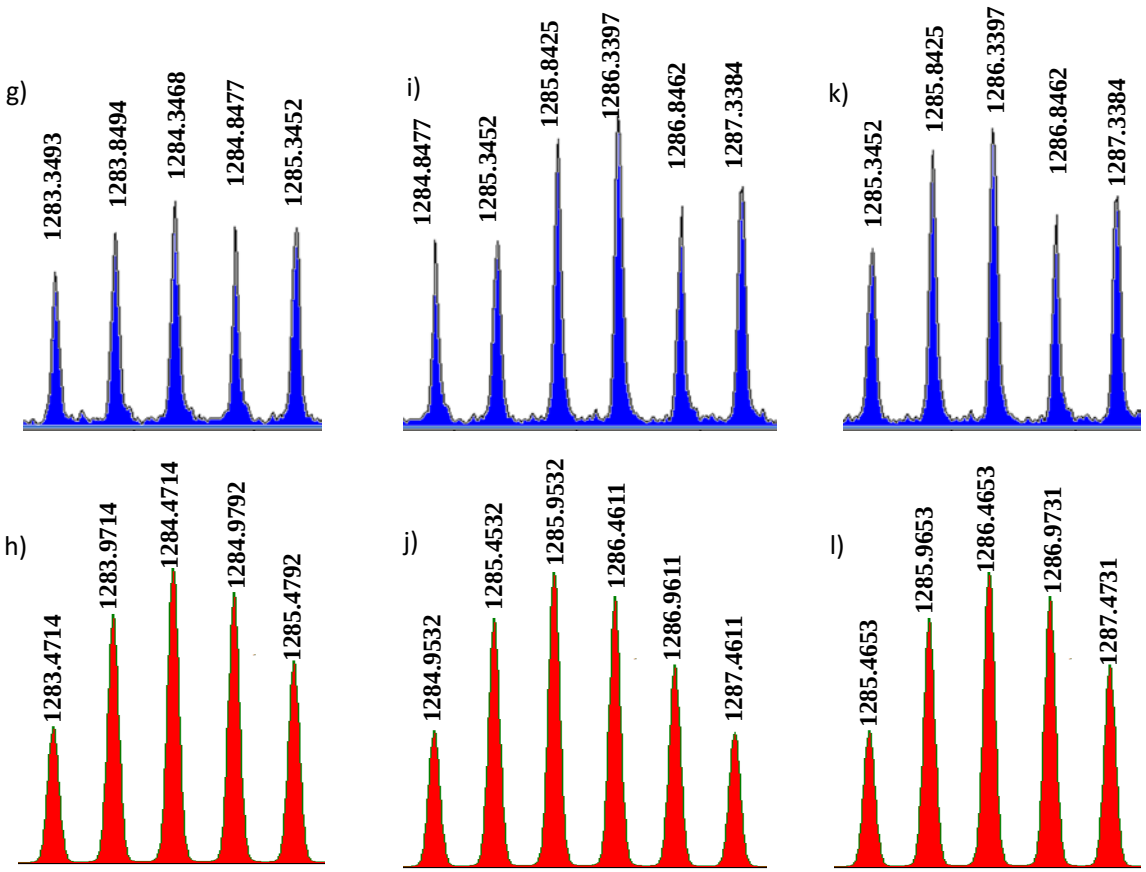

Fig. S21 ESI-MS spectrum of **5**. a) experimental spectrum of [**5** – $2PF_6$]$^{2+}$ (*m*/*z* = 1648.3750) and its fragment [**1b** + **6** + DB24C8 – PF_6]$^{+}$ (*m*/*z* = 1648.3750); b) simulated spectrum of the fragment [**1b** + **6** + DB24C8 – PF_6]$^{+}$; c) simulated spectrum of [**5** – $2PF_6$]$^{2+}$; d) experimental spectrum of [**5** – 2OTf]$^{2+}$ (*m*/*z* = 1644.3840) and its fragment [**1b** + **6** + DB24C8 – OTf]$^{+}$ (*m*/*z* = 1644.3837); e) simulated spectrum of the fragment [**1b** + **6** + DB24C8 – OTf]$^{+}$; f) simulated spectrum of [**5** – 2OTf]$^{2+}$; g) experimental spectrum of [**5** – $3HPF_6$ – 4HOTf + H + NH_4]$^{2+}$ (*m*/*z* = 1283.8494); h) simulated spectrum of [**5** – $3HPF_6$ – 4HOTf + H + NH_4]$^{2+}$ (*m*/*z* = 1283.9714); i) experimental spectrum of [**5** – $4HPF_6$ – 3HOTf + H + NH_4]$^{2+}$ (*m*/*z* = 1285.8425); j) simulated spectrum of [**5** – $4HPF_6$ – 3HOTf + H + NH_4]$^{2+}$ (*m*/*z* = 1285.9532); k) experimental spectrum of [**5** – $3HPF_6$ – 4HOTf + H + Na]$^{2+}$ (*m*/*z* = 1286.3397); l) simulated spectrum of [**5** – $3HPF_6$ – 4HOTf + H + Na]$^{2+}$ (*m*/*z* = 1286.4653).

*7. Investigation of the host-guest complexation DB24C8⊃**1a**, DB30C10⊃**1a** and DB24C8⊃**1b***

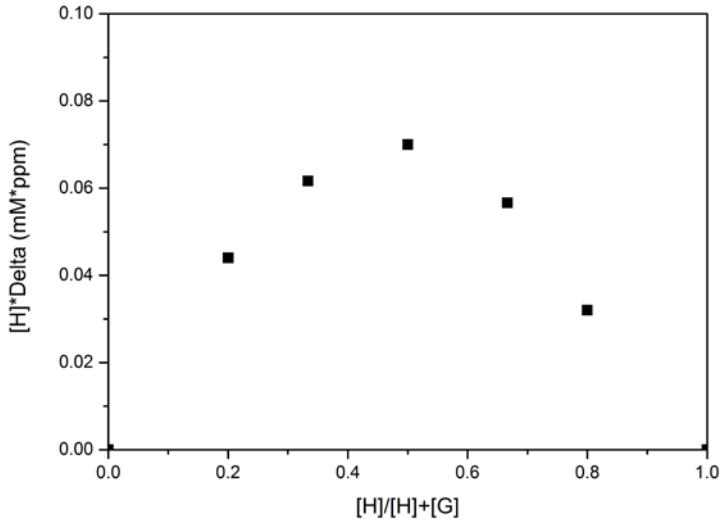

Fig. S22 Job plot showing the 1:1 stoichiometry of the complex between **DB24C8** and the guest **1a** using ^{1}H NMR data of H^{2} on **DB24C8**. [**DB24C8**]$_0$ + [**1a**]$_0$ = 5.00 mM in CD_3COCD_3. [**DB24C8**]$_0$ and [**1a**]$_0$ are initial concentrations of **DB24C8** and **1a**.

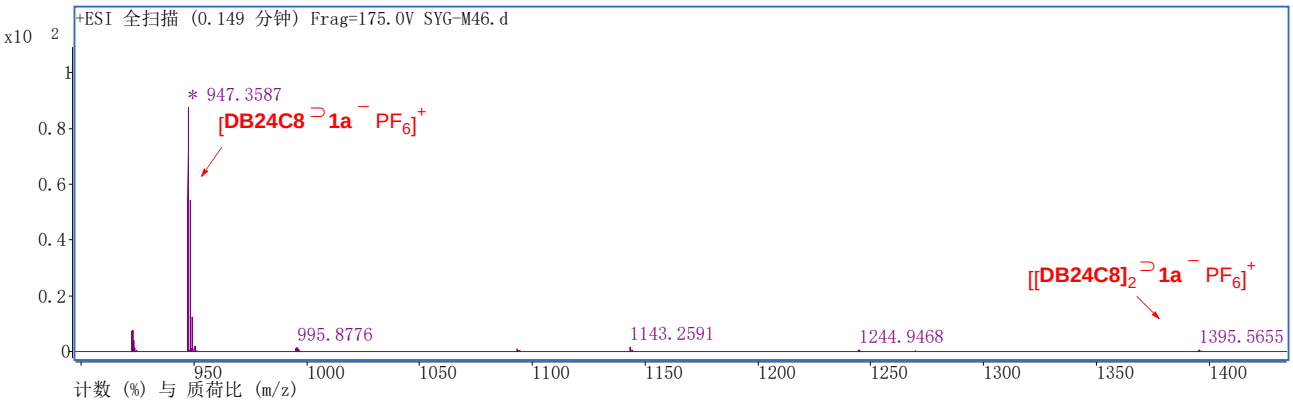

Fig. S23 HRESI mass spectrum of a mixed solution of **1a** and **DB24C8** (1:1 molar ratio). *m*/*z* = 947.3587 for [**DB24C8⊃1a** – PF_6]$^+$, and *m*/*z* = 1395.5655 for [(**DB24C8**)$_2$⊃**1a** – PF_6]$^+$.

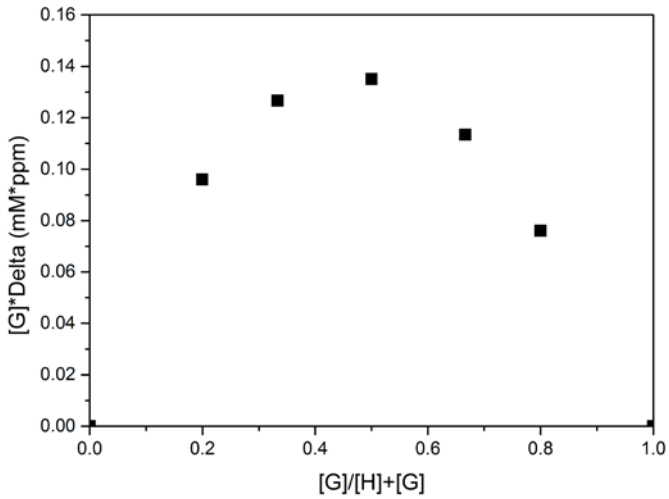

Fig. S24 Job plot showing the 1:1 stoichiometry of the complex between **DB30C10** and the guest **1a** using ^{1}H NMR data of H^{b} on **1a**. [**DB30C10**]$_0$ + [**1a**]$_0$ = 5.00 mM in CD_3COCD_3. [**DB30C10**]$_0$ and [**1a**]$_0$ are initial concentrations of **DB30C10** and **1a**.

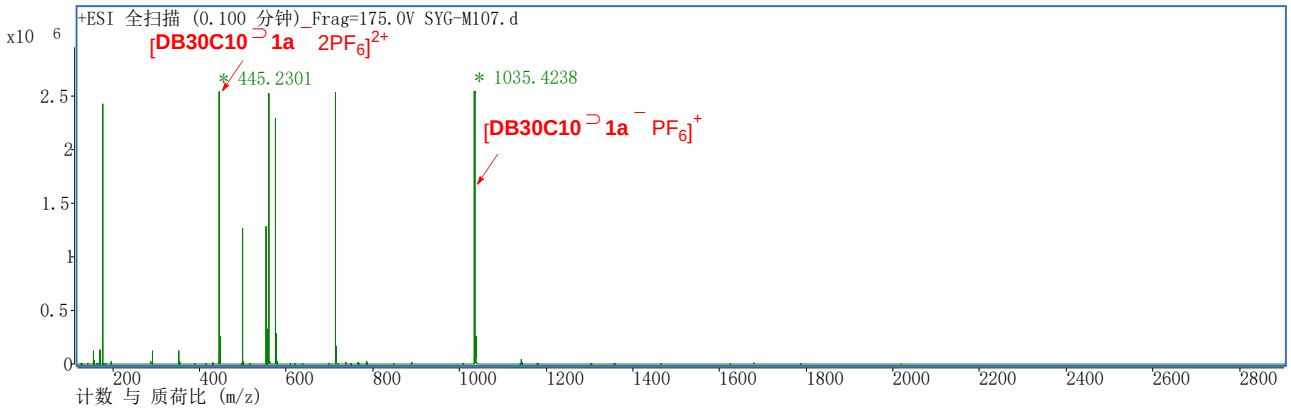

Fig. S25 HRESI mass spectrum of a mixed solution of **1a** and **DB30C10** (1:1 molar ratio). *m*/*z* = 1035.4238 for [**DB30C10⊃1a** – PF_6]$^{+}$, and *m*/*z* = 445.2301 for [**DB30C10⊃1a** – $2PF_6$]$^{2+}$.

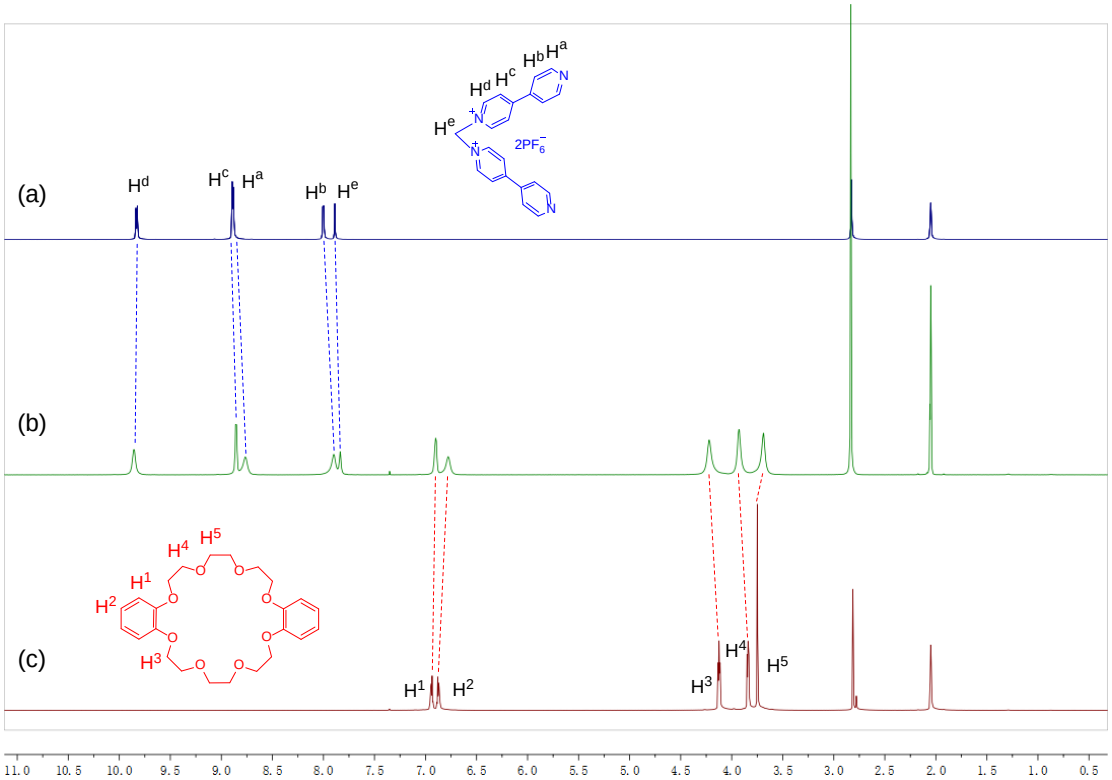

Fig. S26 ^{1}H NMR (500 MHz, acetone-d_6, 25 °C) spectrum of (a) 12.00 mM **1b**, (b) 12.00 mM **1b** + 12.00 mM **DB24C8**, (c) 12.00 mM **DB24C8**.

8. Determination of binding constant (K_a) using the UV-vis titration method

Procedures for UV-vis titration: A 0.04 mM solution of guest **1a** in acetonitrile, and a solution of host (DB24C8 or DB30C10, 20 mM) with guest **1a** (0.04 mM) in acetonitrile were separately prepared. The guest solution (2 mL) was then titrated with the concentrated host solution that contained the guest. Upon each addition, the solution was balanced for more than 1 min before recording the spectrum. The error involved was assumed to be negligible owing to the total change in concentration of the host was small over the course of the titration. The association constants were determined by using the nonlinear least squares fitting of the titration curves and plotting the absorbance A at the host-guest complex charge-transfer band against the concentration of the host. The titration curve was well fitted to the expression of a 1:1 binding isotherm.

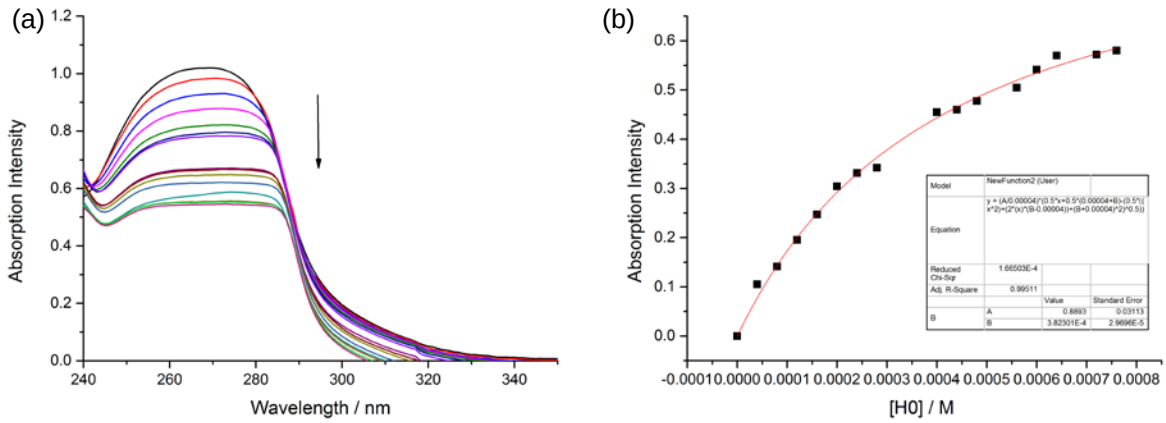

Fig. S27 (a) The absorption spectral changes of **1a** (0.04 mM) upon the addition of **DB24C8** and (b) the absorption intensity changes at λ = 270 nm upon the addition of **DB24C8**.

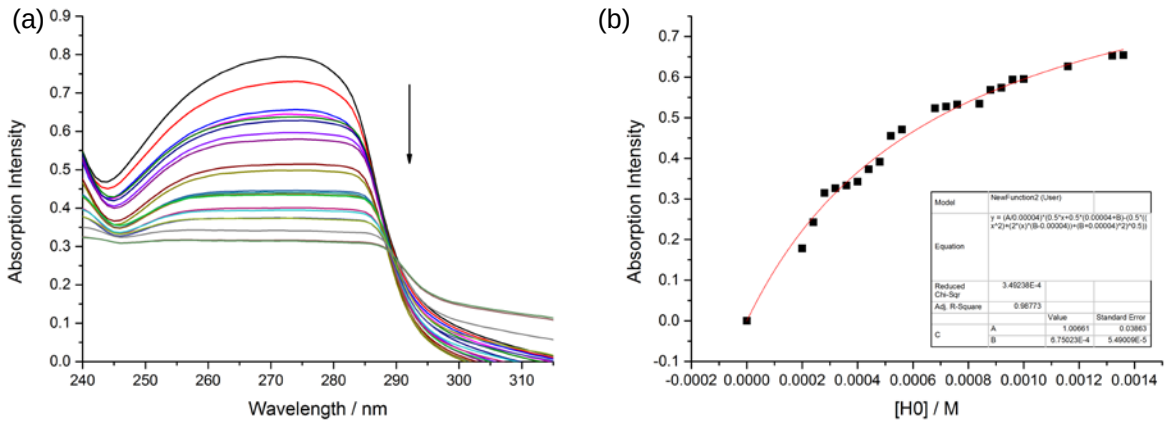

Fig. S28 (a) The absorption spectral changes of **1a** (0.04 mM) upon the addition of **DB30C10** and (b) the absorption intensity changes at λ = 270 nm upon the addition of **DB30C10**.

*9. Crystal structure of **1b***

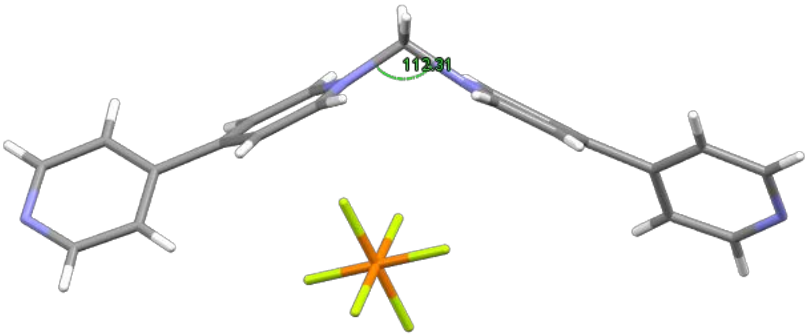

Fig. S29 Crystal structure of 1,1-bis(bipyridinium)methane **1b** reported by Peinador et al. (*J. Am. Chem. Soc.*, 2007, **129**, 13978–13986.)

10. NMR spectra of [3]catenanes by using one-pot construction method

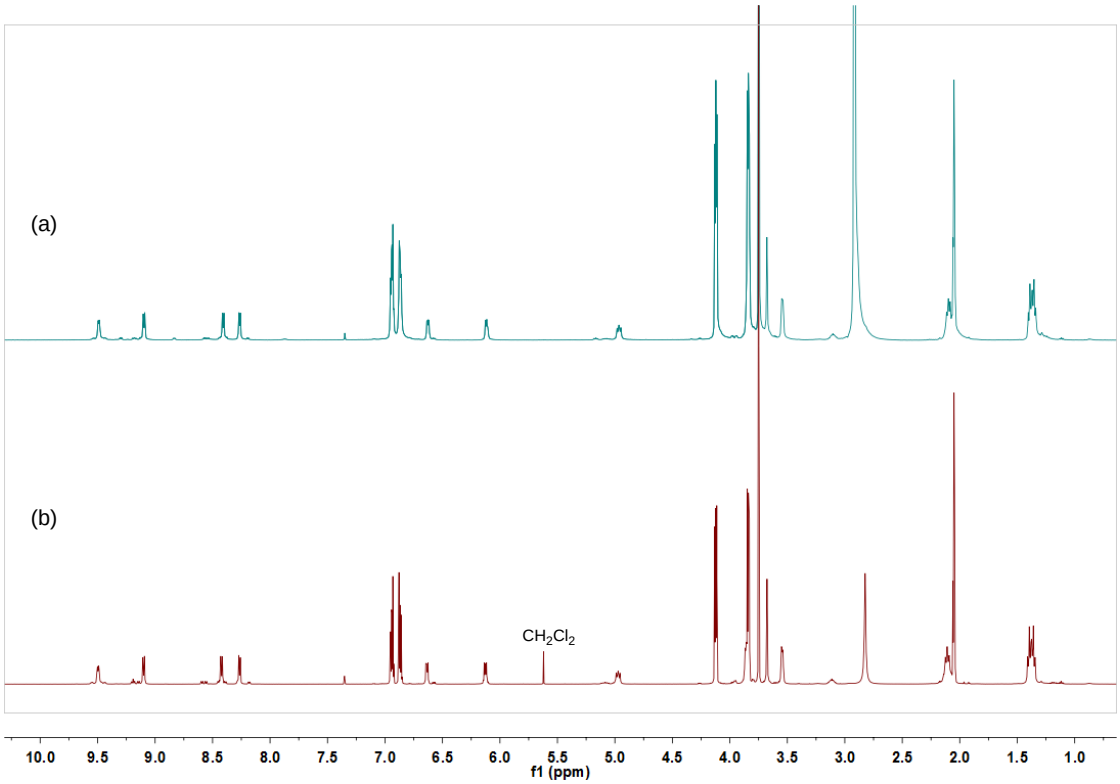

Fig. S30 ^{1}H NMR spectra (500 MHz, acetone-d_6, 25 °C) of [3]catenane **3** (a) self-assembly followed by threading (**2a** + DB24C8), (b) one-pot reaction (**1a** + **6** + DB24C8).

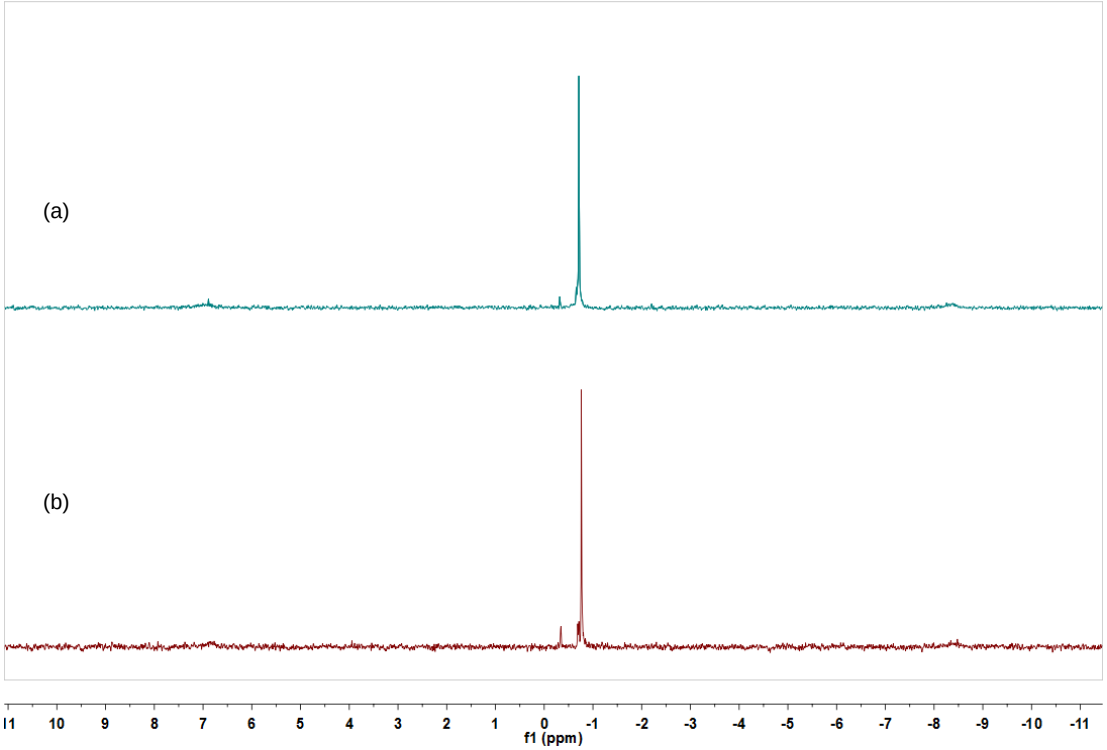

Fig. S31 $^{31}P\{^{1}H\}$ NMR spectra (202 MHz, acetone-d_6, 25 °C) of [3]catenane **3** (a) self-assembly followed by threading (**2a** + DB24C8), (b) one-pot reaction (**1a** + **6** + DB24C8).

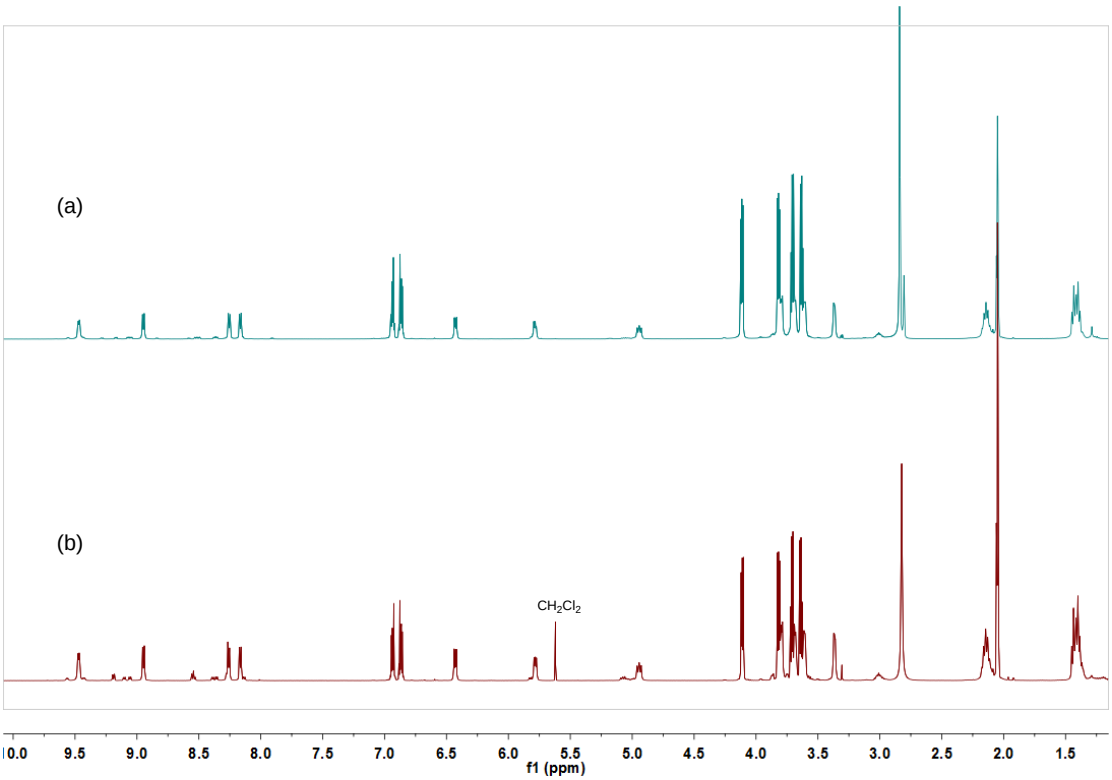

Fig. S32 ^{1}H NMR spectra (500 MHz, acetone-d_6, 25 °C) of [3]catenane **4** (a) self-assembly followed by threading (**2a** + DB30C10), (b) one-pot reaction (**1a** + **6** + DB30C10).

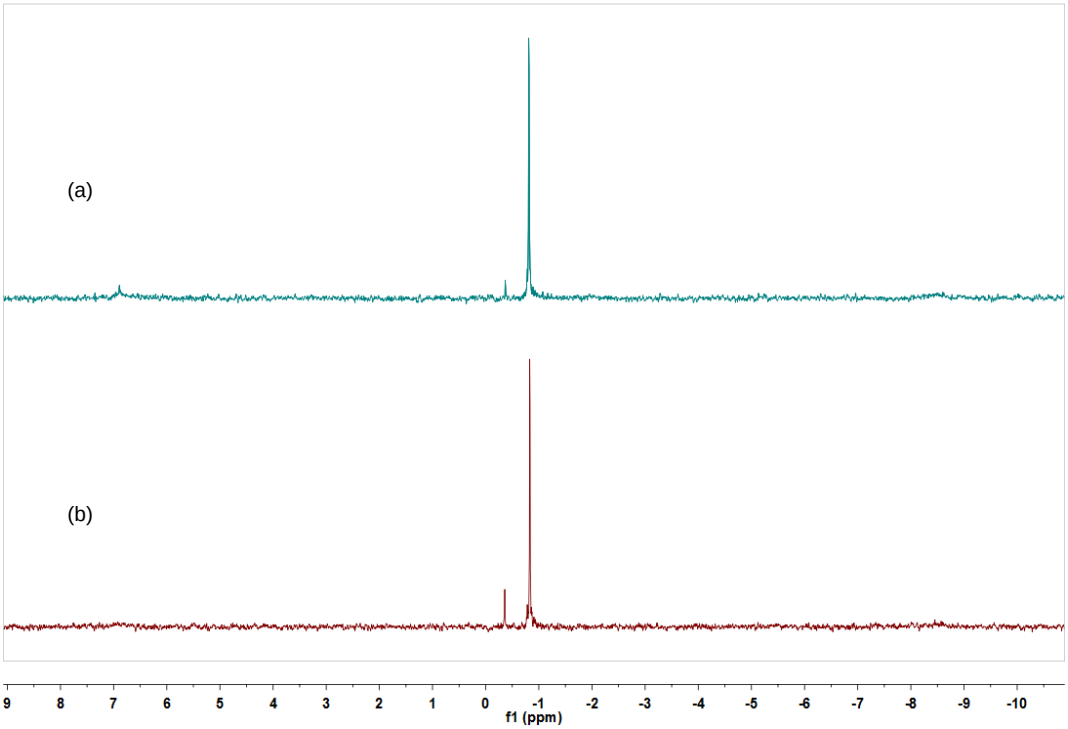

Fig. S33 $^{31}P\{^{1}H\}$ NMR spectra (202 MHz, acetone-d_6, 25 °C) of [3]catenane **4** (a) self-assembly followed by threading (**2a** + DB30C10), (b) one-pot reaction (**1a** + **6** + DB30C10).

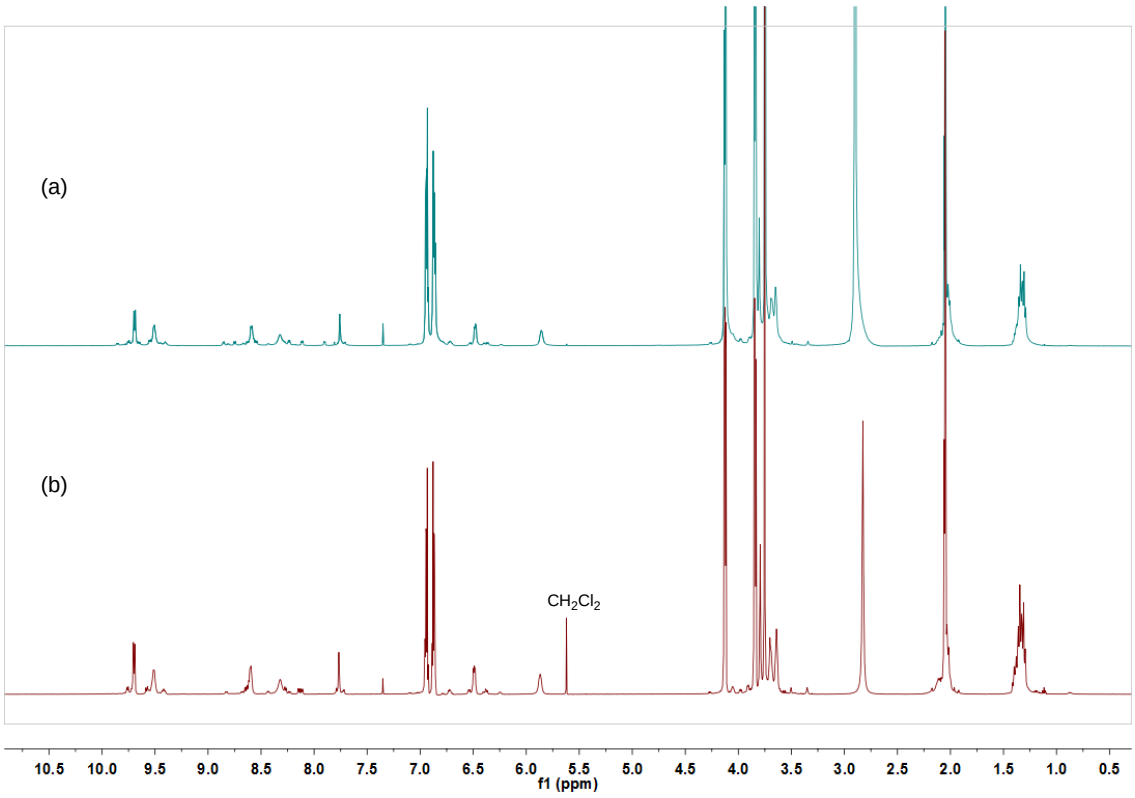

Fig. S34 ^{1}H NMR spectra (500 MHz, acetone-d_6, 25 °C) of [3]catenane **5** (a) self-assembly followed by threading (**2b** + DB24C8), (b) one-pot reaction (**1b** + **6** + DB24C8).

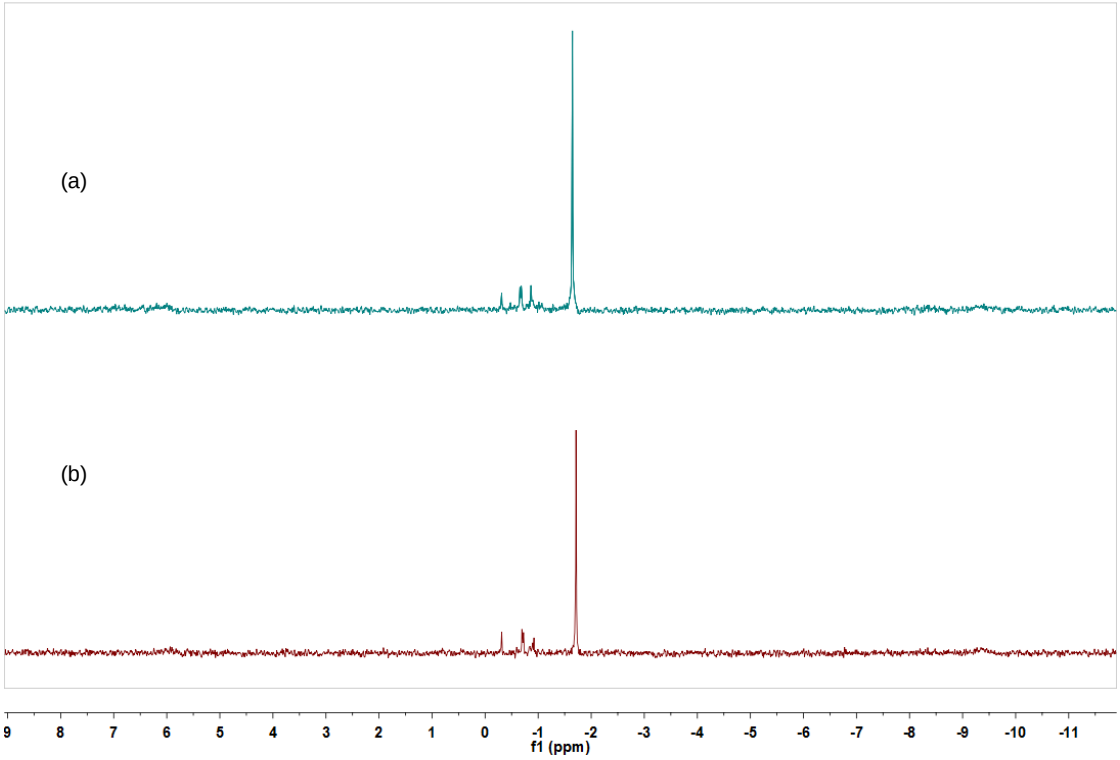

Fig. S35 $^{31}P\{^{1}H\}$ NMR spectra (202 MHz, acetone-d_6, 25 °C) of [3]catenane **5** (a) self-assembly followed by threading (**2b** + DB24C8), (b) one-pot reaction (**1b** + **6** + DB24C8).

*11. Synthesis and characterization of anion-exchanged metallacycles **7**, **8** and [3]catenanes **9**, **10**, **11***

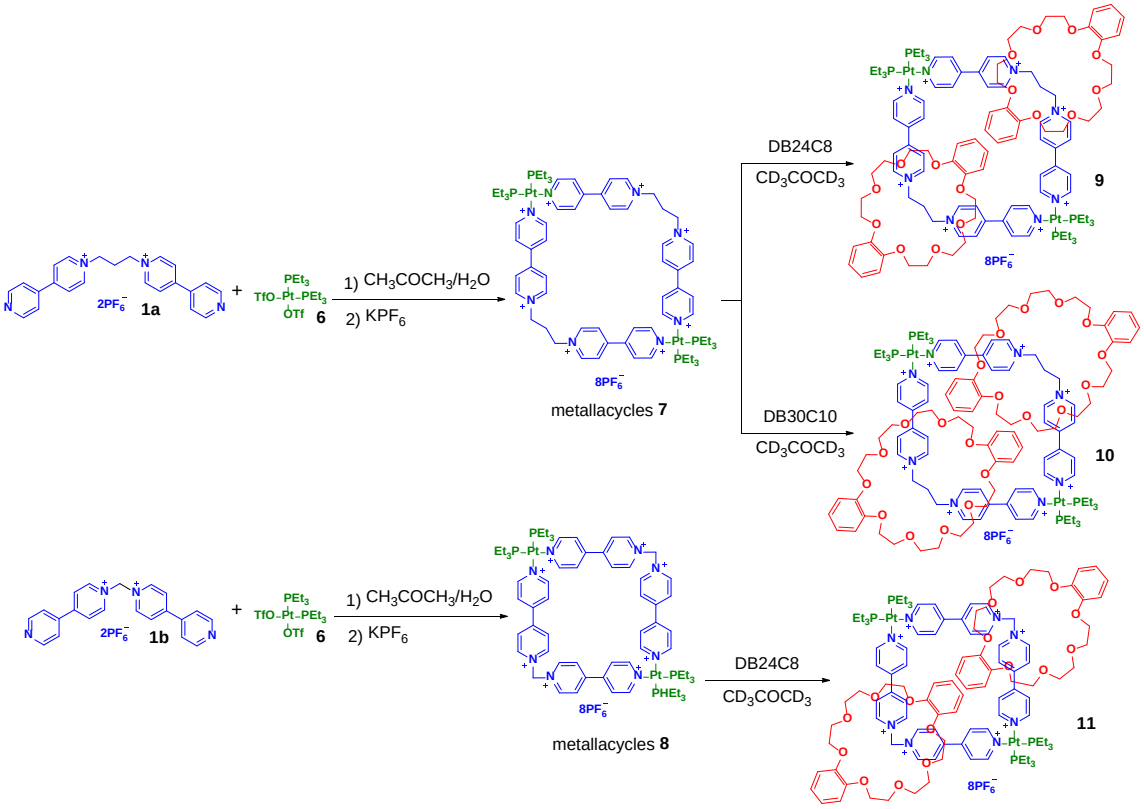

1,3-Bis(4,4'-bipyridinium)propane **1a** or 1,1-bis(4,4'-bipyridinium)methane **1b** (0.012 mmol) and 90° platinum(II) receptor **6** (0.012 mmol) were placed in a 2-dram vial, followed by addition of acetone (1.2 mL) and water (0.4 mL), the solutions were then stirred for 6 h at room temperature. A little excess KPF_6 in aqueous solution was added into the reaction mixture. Acetone was removed by N_2 flow. The resulted precipitate was collected by filtration and the solid was then re-dissolved in acetone (1.0 mL). Water (1.0 mL) was added into the solution and acetone was removed again by N_2 flow. The resulted precipitate was collected by filtration and dried under vacuum to afford metallacycle **7** (15.8 mg, 96%) or **8** (9.3 mg, 58%) as a white solid, respectively.

Corresponding crown ethers (12 mM) were added directly into a solution of metallacycle **7** or **8** (2 mM) in acetone-d_6. The solution was then stirred for 1 days at room temperature to generate [3]catenane (**9**, **10** or **11**). This initial reaction solution was directly used for the following characterization.

Metallacycle **7**: ^{1}H NMR (500 MHz, acetone-d_6,) (Fig. S36): δ (ppm) 9.44 (d, J = 4.8 Hz, 8H), 9.16 (d, J = 7.0 Hz, 8H), 8.53 (d, J = 7.0 Hz, 8H), 8.25 (d, J = 6.6 Hz, 8H), 5.11–5.05 (m, 8H), 2.97–3.03 (m, 4H), 2.11–2.16 (m, 24H), 1.38 (dt, J = 17.6, 7.5 Hz, 36H). ^{31}P{^{1}H} NMR (202 MHz, acetone-d_6) (Fig. S37): δ (ppm) –0.11 (s, ^{195}Pt satellites, $J_{Pt–P}$ = 3110 Hz).

Metallacycle **8**: ^{1}H NMR (500 MHz, acetone-d_6) (Fig. S38): δ (ppm) 9.80 (d, J = 7.1 Hz, 8H), 9.44 (d, J = 4.8 Hz, 8H), 8.64 (d, J = 7.1 Hz, 8H), 8.16 (d, J = 6.6 Hz, 8H), 7.85 (s, 4H), 2.13 (dt, J = 16.0, 7.8 Hz, 24H), 1.41–1.34 (m, 36H). ^{31}P{^{1}H} NMR (202 MHz, acetone-d_6) (Fig. S39): δ (ppm) –0.10 (s, ^{195}Pt satellites, $J_{Pt–P}$ = 3104 Hz).

[3]Catenane **9**: ^{1}H NMR (500 MHz, acetone-d_6) (Fig. S40): δ (ppm) 9.46 (d, J = 4.8 Hz, 8H), 9.10 (d, J = 7.0 Hz, 8H), 8.35 (d, J = 7.0 Hz, 8H), 8.22 (d, J = 6.6 Hz, 8H), 6.61 (dd, J = 6.0, 3.6 Hz, 8H), 6.16 (dd, J = 6.1, 3.4 Hz, 8H), 5.04–4.97 (m, 8H), 3.82 (s, 16H), 3.69 (s, 16H), 3.61–3.52 (m, 16H), 3.19–3.11 (m, 4H), 2.10–2.15 (m, 24H), 1.41–1.35 (m, 36H). ^{31}P{^{1}H} NMR (202 MHz, acetone-d_6) (Fig. S41): δ (ppm) –0.66 (s, ^{195}Pt satellites, $J_{Pt–P}$ = 3112 Hz).

[3]Catenane **10**: ^{1}H NMR (500 MHz, acetone-d_6) (Fig. S42): δ (ppm) 9.44 (d, J = 4.9 Hz, 8H), 8.95 (d, J = 6.8 Hz, 8H), 8.18 (d, J = 6.8 Hz, 8H), 8.11 (d, J = 6.5 Hz, 8H), 6.39 (dd, J = 5.9, 3.6 Hz, 8H), 5.81 (dd, J = 5.9, 3.4 Hz, 8H), 4.99–4.91 (m, 8H), 3.79 (d, J = 5.4 Hz, 16H), 3.69 (d, J = 2.0 Hz,

16H), 3.58 (d, J = 4.8 Hz, 16H), 3.37 (d, J = 2.9 Hz, 16H), 3.04–2.98 (m, 4H), 2.15 (dd, J = 15.9, 7.2 Hz, 25H), 1.44–1.38 (m, 36H). $^{31}P\{^{1}H\}$ NMR (202 MHz, acetone-d_6) (Fig. S43): δ (ppm) –0.69 (s, ^{195}Pt satellites, J_{Pt-P} = 3108 Hz).

[3]Catenane **11**: ^{1}H NMR (500 MHz, acetone-d_6) (Fig. S44): δ (ppm) 9.72 (d, J = 6.7 Hz, 8H), 9.47 (d, J = 4.2 Hz, 8H), 8.54 (d, J = 6.3 Hz, 8H), 8.26 (s, 8H), 7.80 (s, 4H), 6.52–6.41 (m, 8H), 5.89 (s, 8H), 3.80 (s, 16H), 3.68 (d, J = 4.9 Hz, 16H), 3.65 (s, 16H), 2.04–1.96 (m, 24H), 1.36–1.30 (m, 36H). $^{31}P\{^{1}H\}$ NMR (202 MHz, acetone-d_6) (Fig. S45): δ (ppm) –1.65 (s, ^{195}Pt satellites, J_{Pt-P} = 3131 Hz).

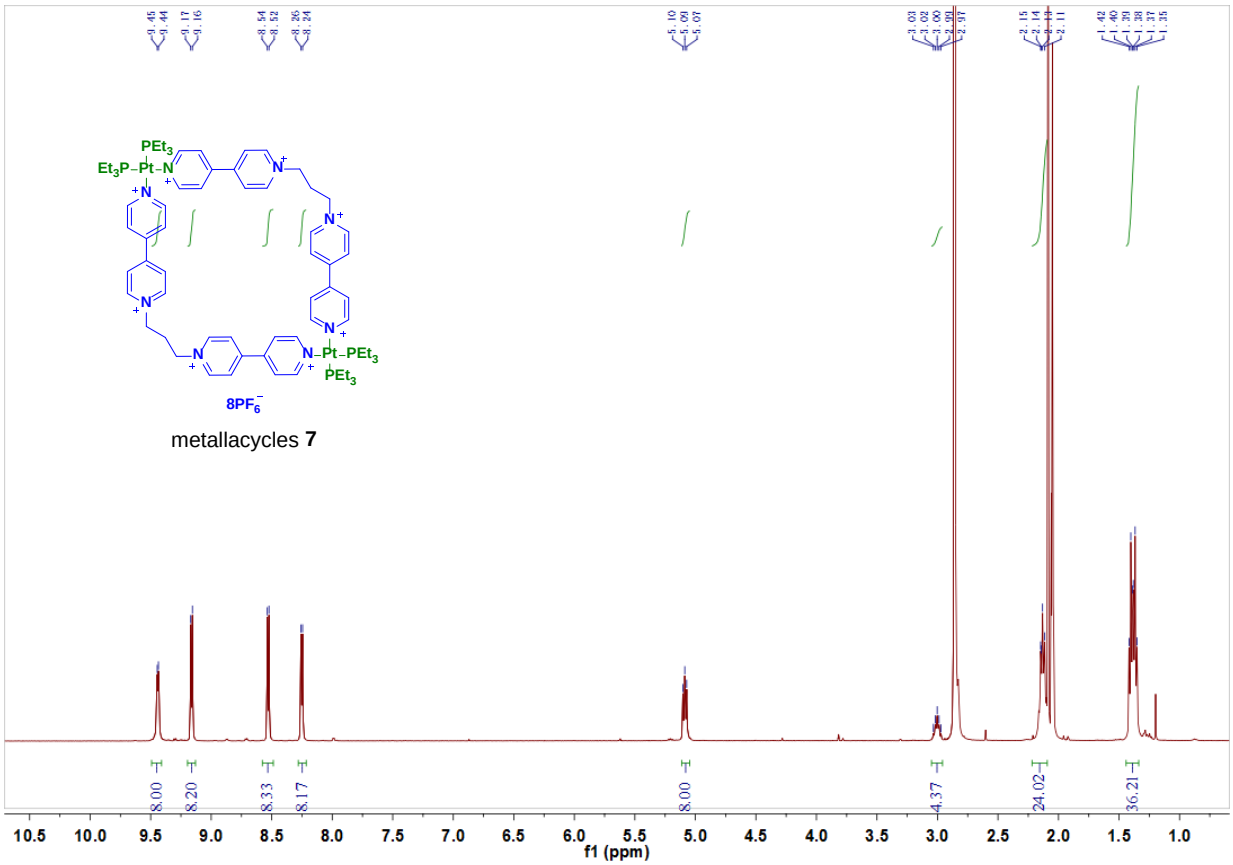

Fig. S36 ^{1}H NMR (500 MHz, acetone-d_6, 25 °C) spectrum of metallacycle **7**.

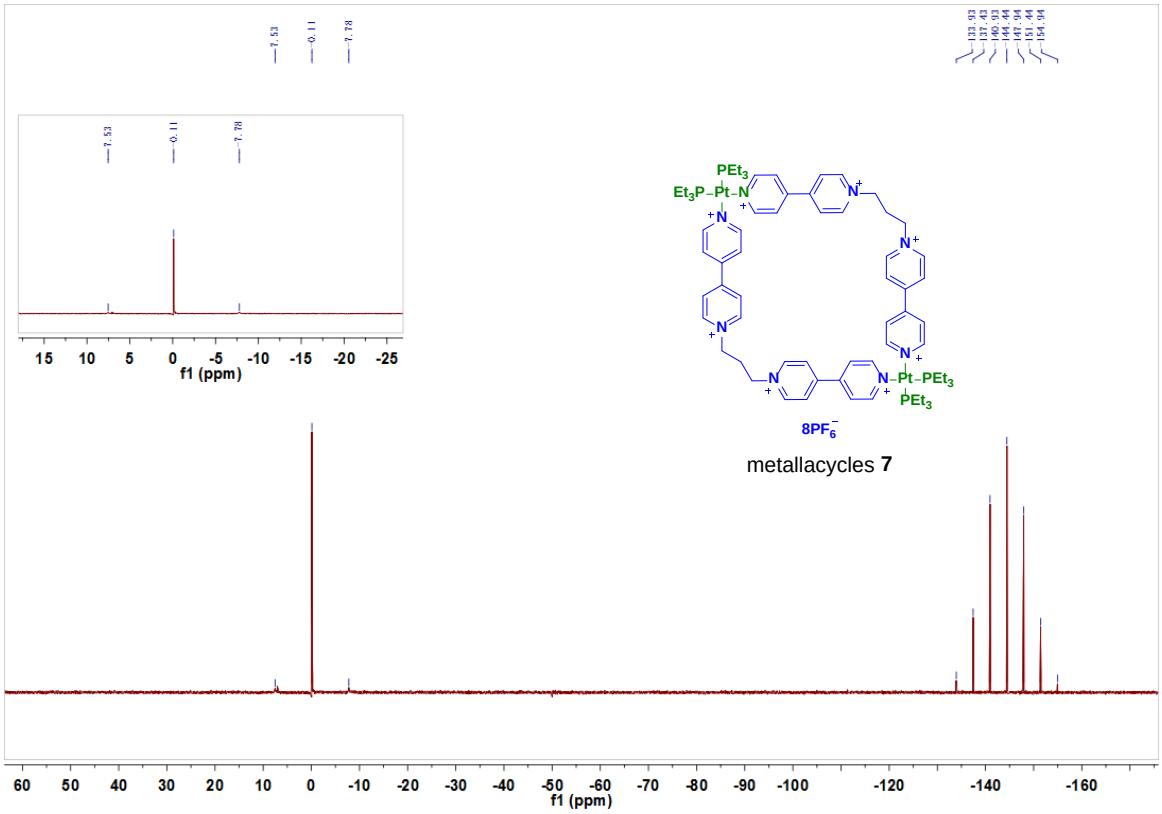

Fig. S37 $^{31}P\{^{1}H\}$ NMR (202 MHz, acetone-d_6, 25 °C) spectrum of metallacycle **7**.

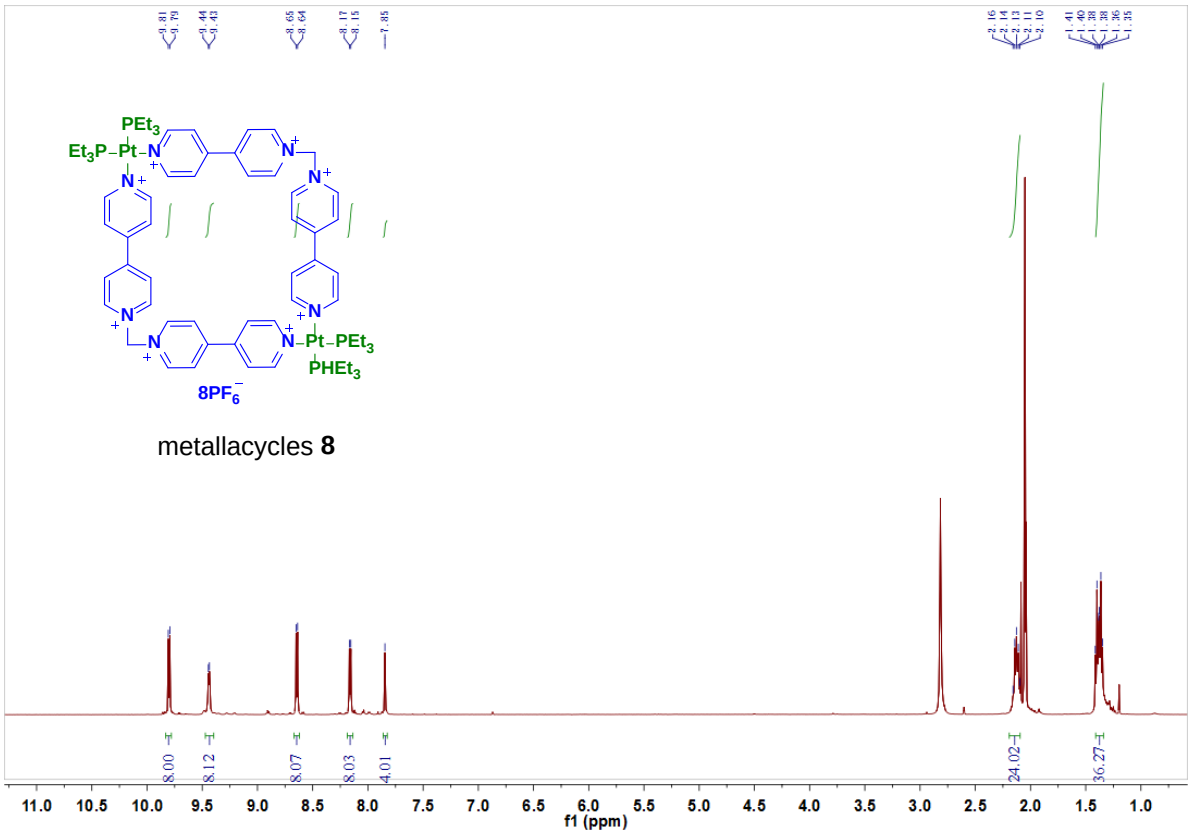

Fig. S38 ^{1}H NMR (500 MHz, acetone-d_6, 25 °C) spectrum of metallacycle **8**.

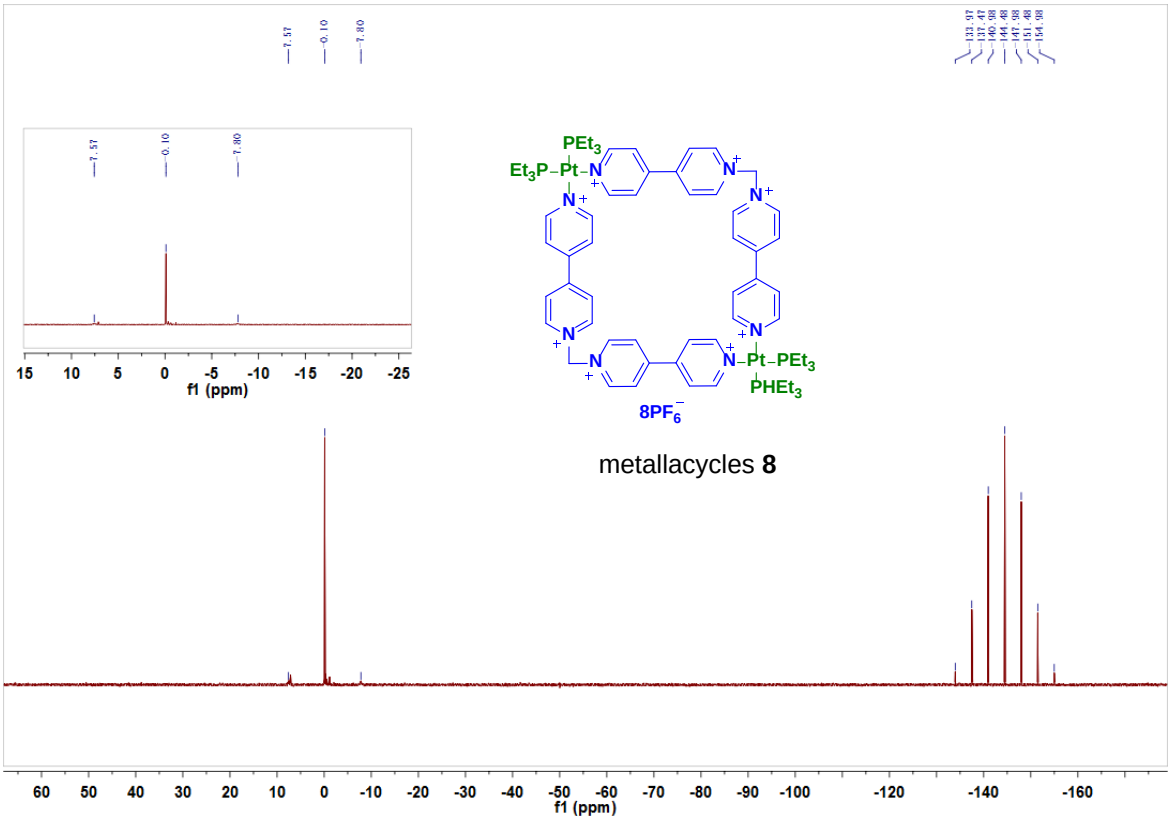

Fig. S39 $^{31}P\{^{1}H\}$ NMR (202 MHz, acetone-d_6, 25 °C) spectrum of metallacycle **8**.

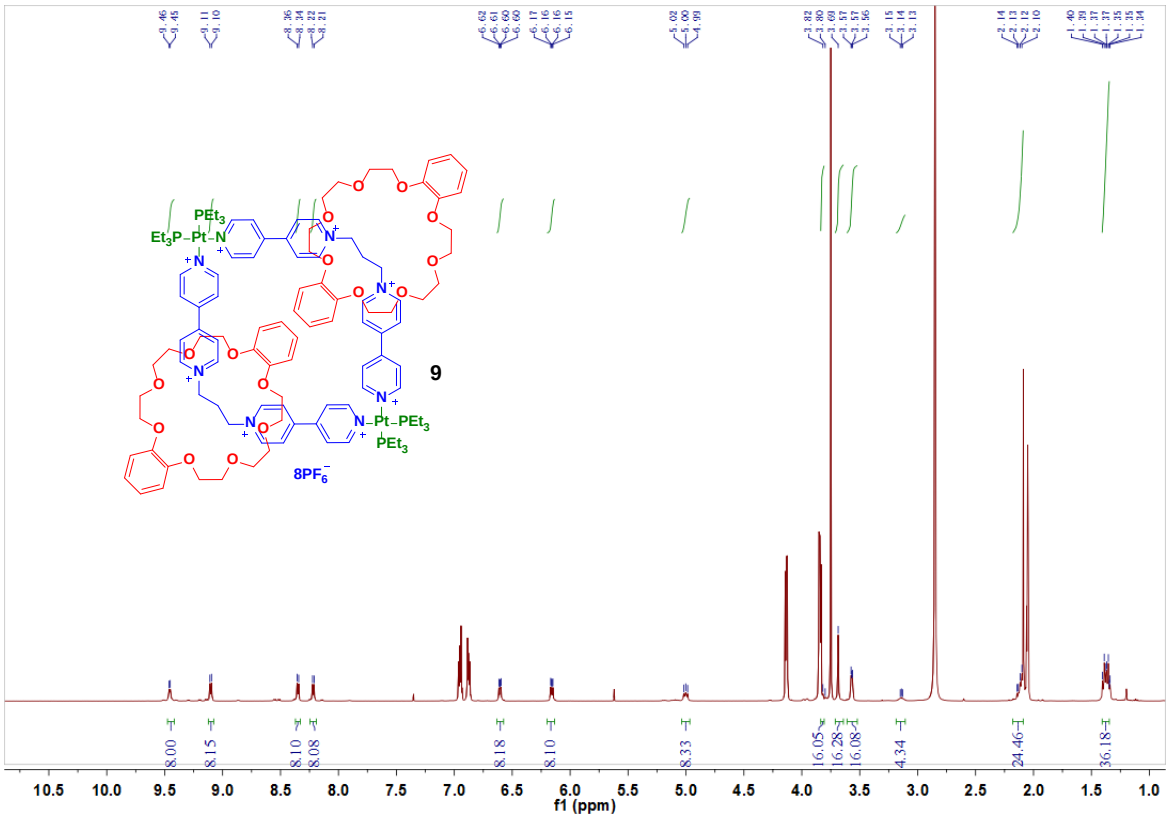

Fig. S40 ^{1}H NMR (500 MHz, acetone-d_6, 25 °C) spectrum of [3]catenane **9**.

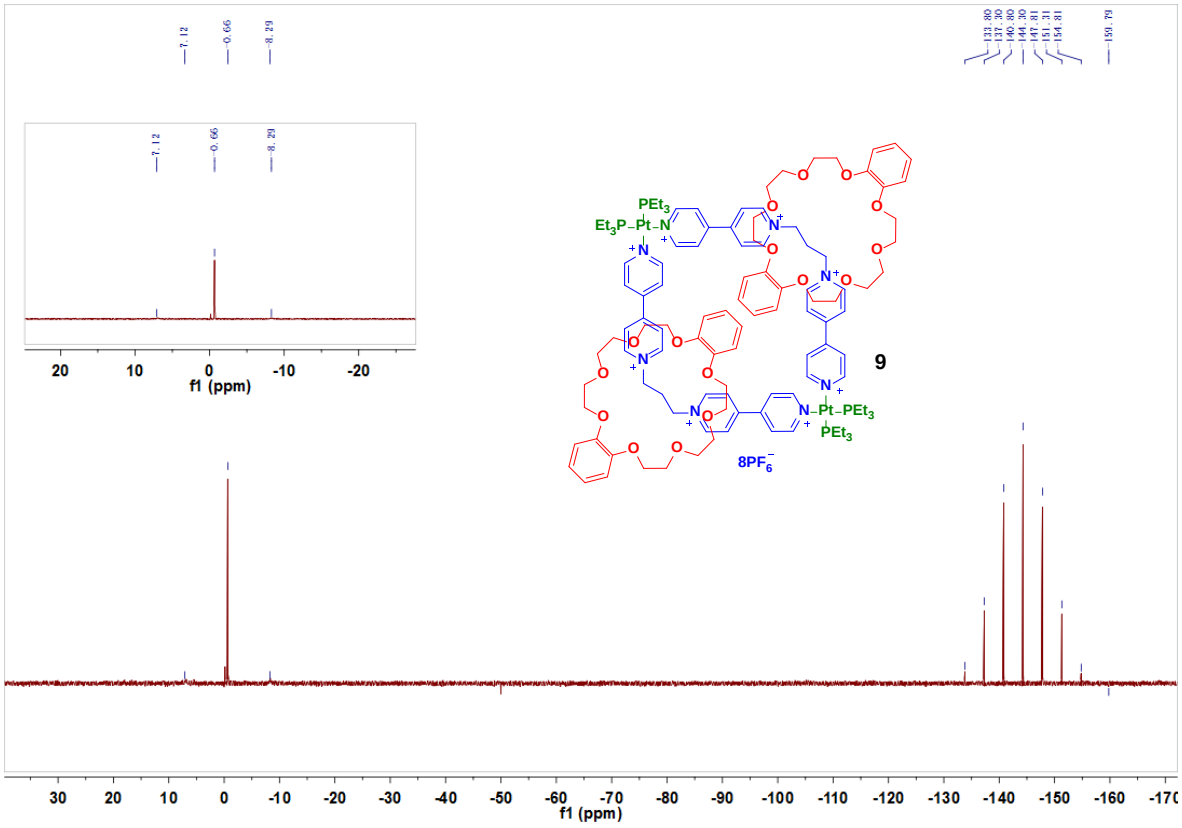

Fig. S41 $^{31}P\{^{1}H\}$ NMR (202 MHz, acetone-d_6, 25 °C) spectrum of [3]catenane **9**.

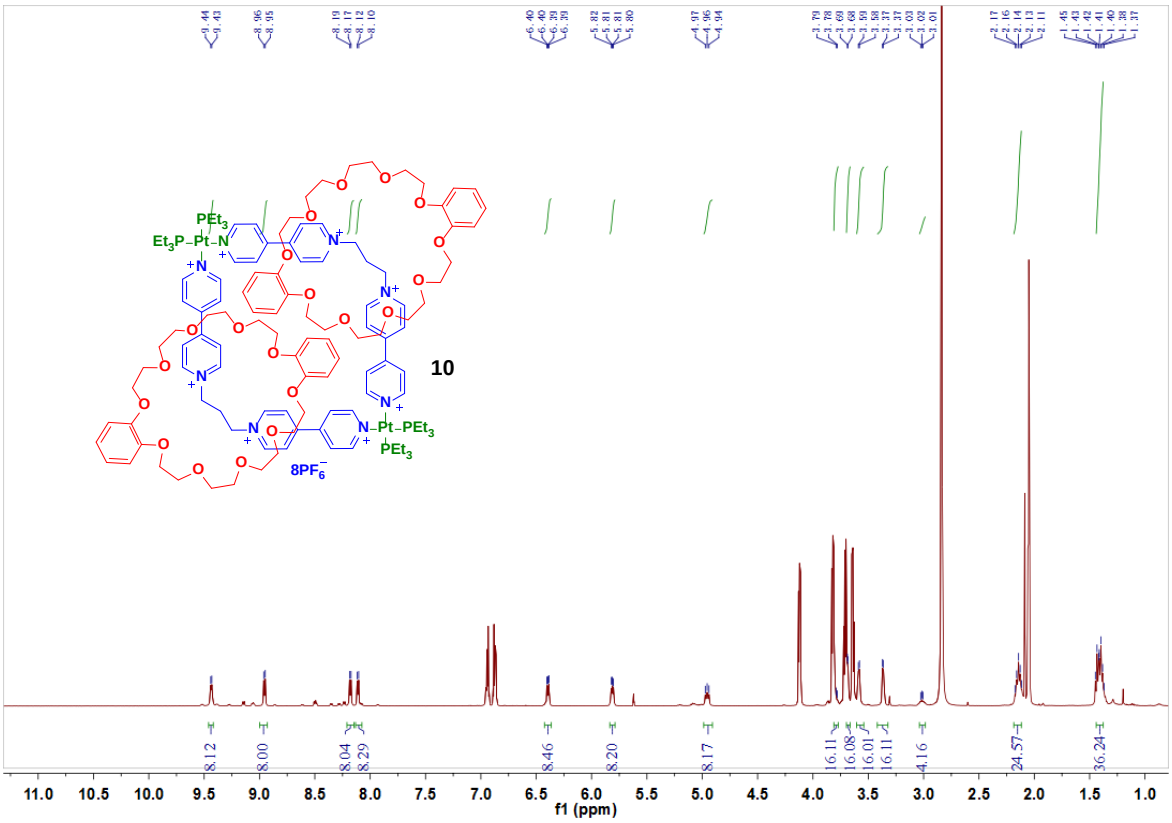

Fig. S42 ^{1}H NMR (500 MHz, acetone-d_6, 25 °C) spectrum of [3]catenane **10**.

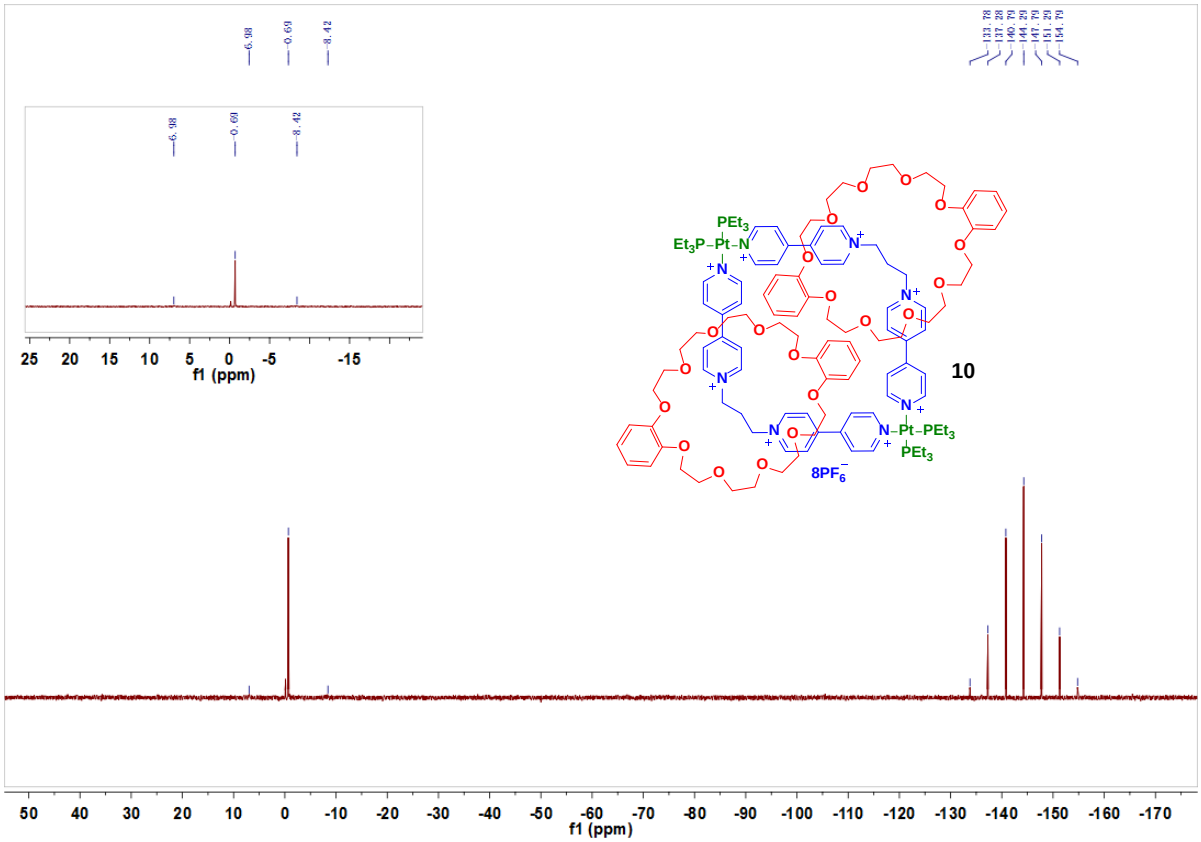

Fig. S43 $^{31}P\{^{1}H\}$ NMR (202 MHz, acetone-d_6, 25 °C) spectrum of [3]catenane **10**.

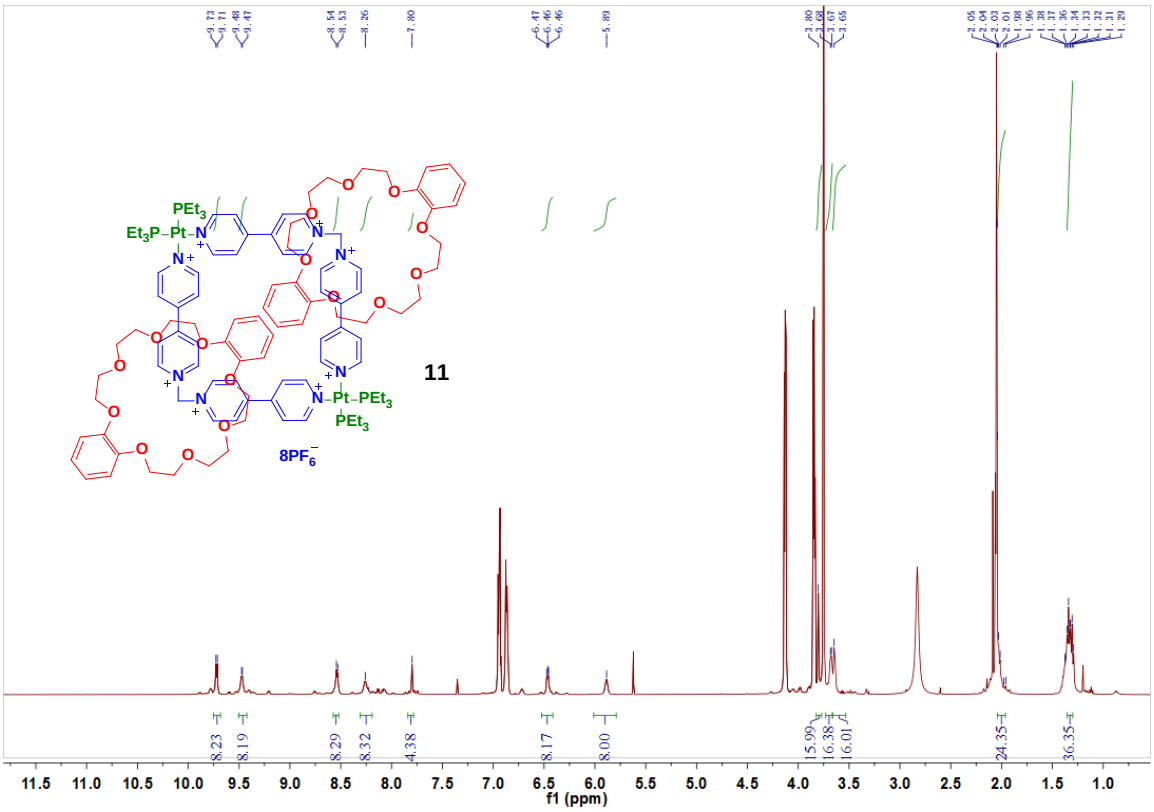

Fig. S44 ^{1}H NMR (500 MHz, acetone-d_6, 25 °C) spectrum of [3]catenane **11**.

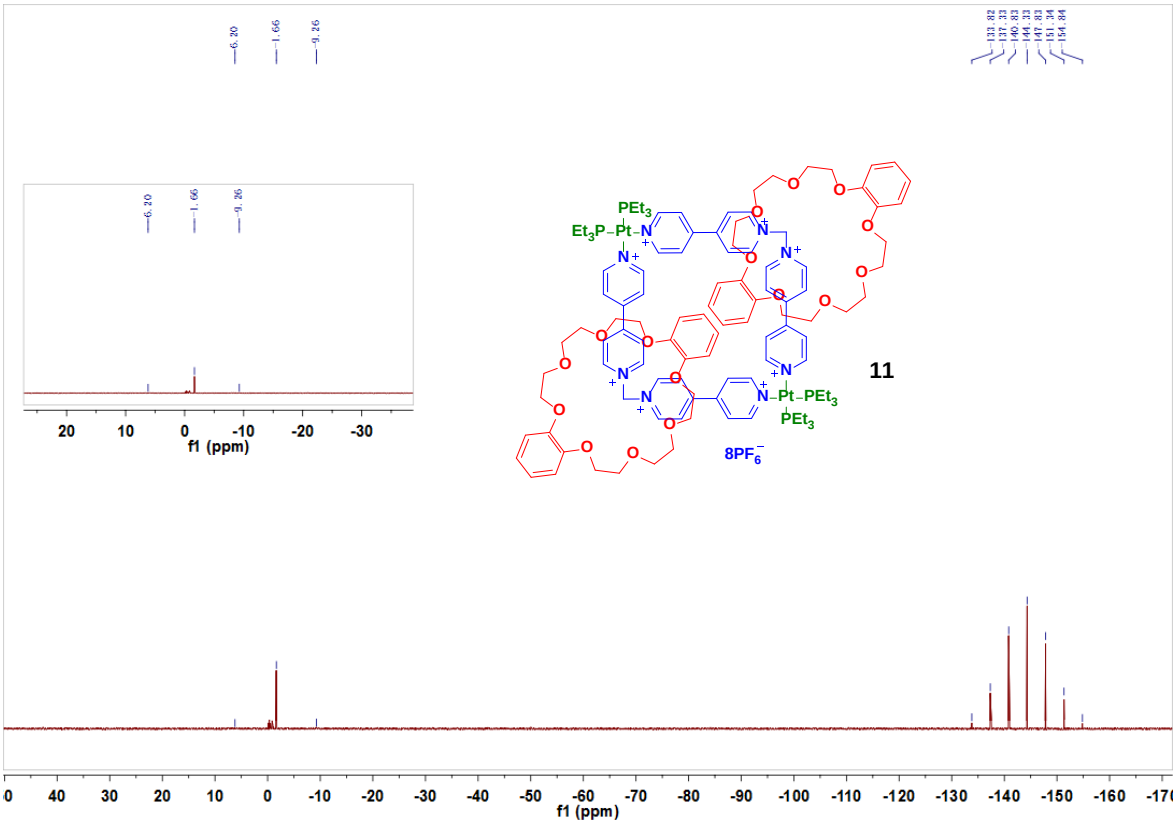

Fig. S45 $^{31}P\{^{1}H\}$ NMR (202 MHz, acetone-d_6, 25 °C) spectrum of [3]catenane **11**.

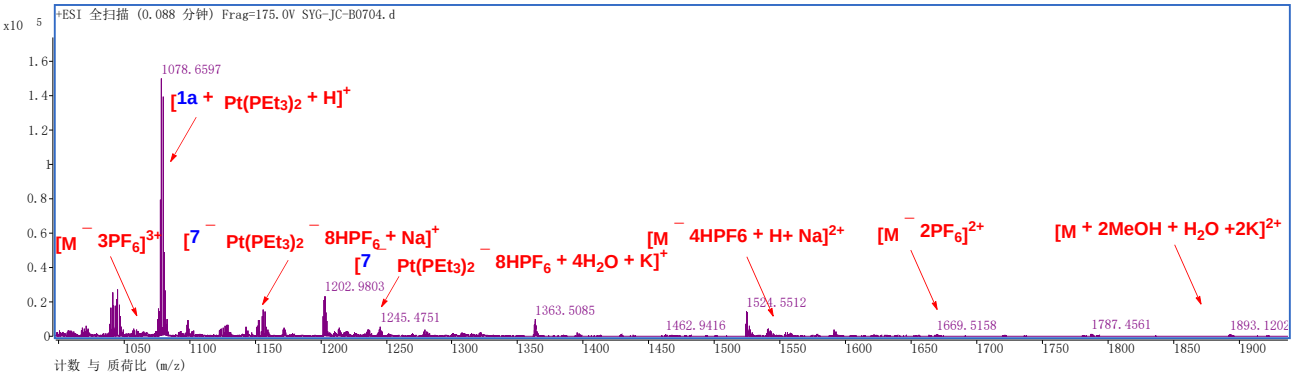

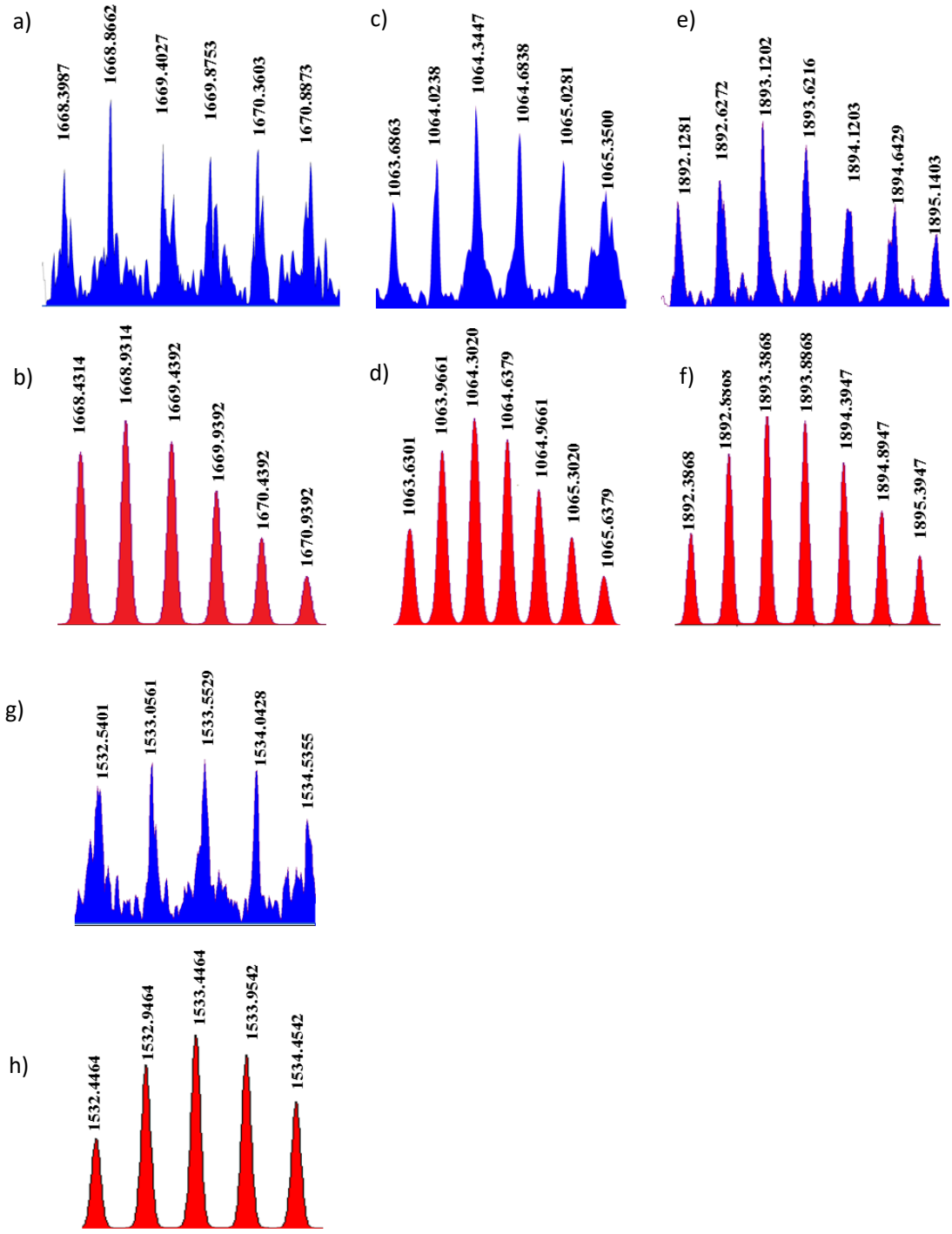

Fig. S46 ESI-MS spectrum of **9**. a) experimental spectrum of [**9** – $2PF_6$]$^{2+}$ (*m/z* = 1668.8662); b) simulated spectrum of [**9** – $2PF_6$]$^{2+}$ (*m/z* = 1668.9314); c) experimental spectrum of [**9** – $3PF_6$]$^{3+}$ (*m/z* = 1064.3447); d) simulated spectrum of [**9** – $3PF_6$]$^{3+}$ (*m/z* = 1064.3020); e) experimental spectrum of [**9** + 2MeOH + H_2O +2K]$^{2+}$ (*m/z* = 1893.1202); f) simulated spectrum of [**9** + 2MeOH + H_2O +2K]$^{2+}$ (*m/z* = 1893.3868); g) experimental spectrum of [**9** – $4HPF_6$ + H+ Na]$^{2+}$ (*m/z* = 1533.5529); h) simulated spectrum of [**9** – $4HPF_6$ + H+ Na]$^{2+}$ (*m/z* = 1533.4464).

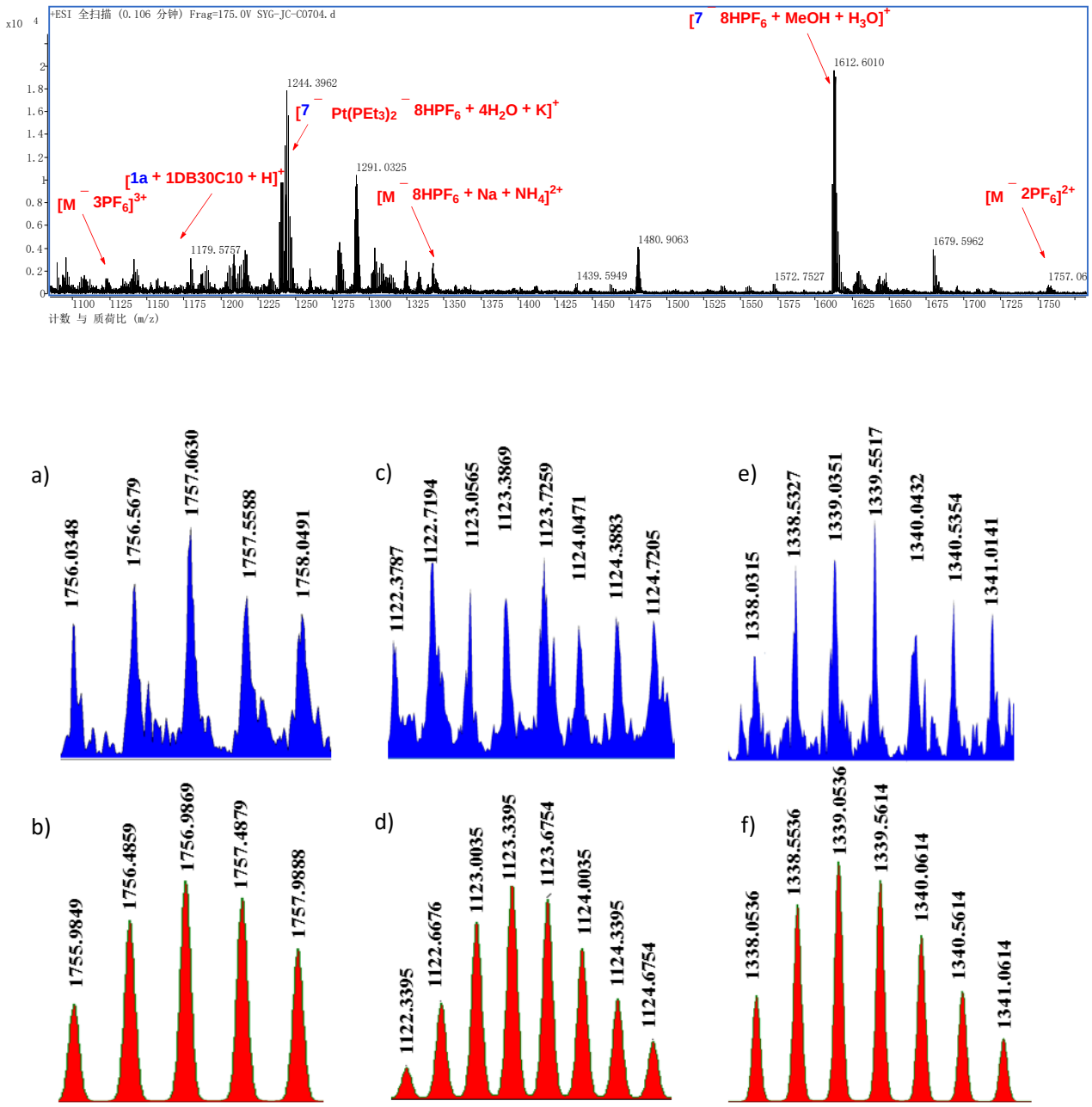

Fig. S47 ESI-MS spectrum of **10**. a) experimental spectrum of [**10** – $2PF_6$]$^{2+}$ (*m*/*z* = 1757.0630); b) simulated spectrum of [**10** – $2PF_6$]$^{2+}$ (*m*/*z* = 1756.9869); c) experimental spectrum of [**10** – $3PF_6$]$^{3+}$ (*m*/*z* = 1122.7149); d) simulated spectrum of [**10** – $3PF_6$]$^{3+}$ (*m*/*z* = 1122.6676); e) experimental spectrum of [**10** – $8HPF_6$ + Na + NH_4]$^{2+}$ (*m*/*z* = 1339.5517); f) simulated spectrum of [**10** – $8HPF_6$ + Na + NH_4]$^{2+}$ (*m*/*z* = 1339.0536).

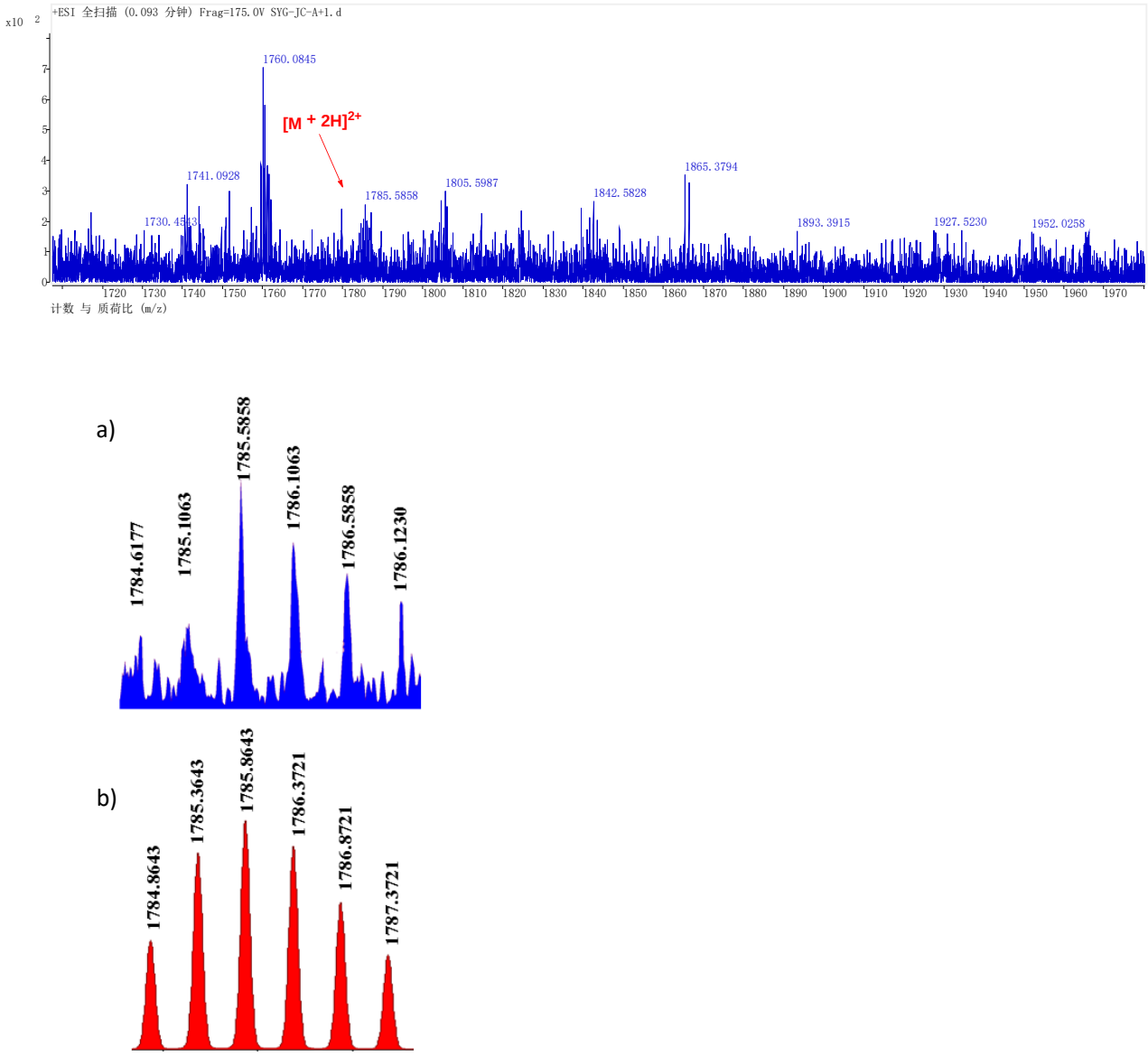

Fig. S48 ESI-MS spectrum of **11**. a) experimental spectrum of [**11** + 2H]$^{2+}$ (*m*/*z* = 1785.5858); b) simulated spectrum of [**11** + 2H]$^{2+}$ (*m*/*z* = 1785.8643).

*12. X-ray analysis data of **1a** and [3]catenane **4***

Compounds	Guest **1a**	[3]catenane **4**
Empirical formula	$C_{23}H_{22}F_{12}N_4P_2$	$C_{126}H_{184}F_{48}N_8O_{20}P_{12}Pt_2$
Formula weight	644.38	3804.62
Temperature [K]	170.0	170.0
Crystal system	Monoclinic	Triclinic
Space group	$P2_1/c$	P-1
a [Å]	7.1855(5)	10.1341(4)
b [Å]	14.1620(8)	21.2668(8)
c [Å]	25.8378(19)	22.2187(9)
α [°]	90	62.6960(10)
β [°]	90.229(2)	78.8210(10)
γ [°]	90	76.6310(10)
Volume [Å^3]	2629.3(3)	4118.3(3)
Z	4	1
Density [Mg/m^3]	1.628	1.534
Absorption coefficient [mm^{-1}]	0.273	1.927
F [000]	1304.0	1924.0
Crystal size [mm^3]	0.36 × 0.18 × 0.07	0.42 × 0.16 × 0.12
Radiation	MoKα (λ = 0.71073)	MoKα (λ = 0.71073)
2θ range for data collection [°]	4.268 to 64.622	4.148 to 54.276
Index ranges	$-10 \leqslant h \leqslant 10$, $-21 \leqslant k \leqslant 21$, $0 \leqslant l \leqslant 38$	$-12 \leqslant h \leqslant 12$, $-27 \leqslant k \leqslant 27$, $-28 \leqslant l \leqslant 28$
Reflections collected	8371	101992
Independent reflections	8371 [Rint = ?, Rsigma = 0.0633]	18164 [R_{int} = 0.0464, R_{sigma} = 0.0321]
Data/restraints/parameters	8371/6/426	18164/39/1010
Goodness-of-fit on F^2	1.021	1.018
Final R indexes [$I > 2\sigma(I)$]	R_1 = 0.0743, wR_2 = 0.1856	R_1 = 0.0483, wR_2 = 0.1220
Final R indexes (all data)	R_1 = 0.1175, wR_2 = 0.2196	R_1 = 0.0624, wR_2 = 0.1331
Largest diff. peak and hole [e.Å^{-3}]	0.91/–0.63	1.68/–1.61
Deposition Number	**2079026**	**2079027**